Supporting Information for:

The formation of highly oxidized multifunctional products in the ozonolysis of cyclohexene

Matti P. Rissanen*[1], Theo Kurtén[2], Mikko Sipilä[1], Joel A. Thornton[3], Juha Kangasluoma[1], Nina Sarnela[1], Heikki Junninen[1], Solvejg Jørgensen[4], Simon Schallhart[1], Maija K. Kajos[1], Risto Taipale[1], Taina Ruuskanen[1], Tuukka Petäjä[1], Douglas R. Worsnop[5], Henrik G. Kjaergaard[4] and Mikael Ehn[1]

[1]Department of Physics, P.O. Box 64, 00014 University of Helsinki, Finland.
[2]Department of Chemistry, P.O. Box 55, 00014 University of Helsinki, Finland.
[3]Department of Atmospheric Sciences, University of Washington, Seattle, WA 98195, USA.
[4]Department of Chemistry, University of Copenhagen, Universitetsparken 5, 2100 Copenhagen Ø, Denmark.
[5]Aerodyne Research Inc., 45 Manning Road, Billerica, MA 01821, USA.

S1. Experimental

S1.1. Laboratory investigations

The CI-APi-TOF mass spectrometer (Tofwerk AG, Switzerland), the nitrate chemical ionization scheme and the measurement routines have been described previously[62, 63]. Briefly, the atmospheric pressure sample is introduced to the chemical ionization inlet by 3/4-inch stainless steel tube. In the CI-inlet, sheath flow carries the charged nitrate clusters and an applied electric field introduces the ions into the sample gas flow. The charging is brought about (mainly) by nitrate dimers (i.e., $HNO_3*NO_3^-$), and adducts between sample molecules and the NO_3^- ion form if the bond between the sample molecule and NO_3^- is stronger than the bond between HNO_3 and NO_3^-. Contrary to a previous publication[62] the ionizing radiation in the CI-inlet was provided by a Hamamatsu L9490 soft X-ray photoionizer, which has been tested against the more commonly applied Americium 241 radioactive charger and has been found to give consistent results.

The ozonolysis reactions (C_6H_{10}, C_6D_{10} and *cis*-6-nonenal) were investigated in two borosilicate glass flow tube reactors (205 cm long/4.7 cm i.d. and 63 cm long/4.0 cm i.d.) coupled to a nitrate CI-APi-TOF mass spectrometer (see Figure S1). The reagents were brought into the flow tubes with 0.4 cm i.d. Nylon or Teflon tubing, connected to the reactor by a 1 cm i.d. cross Swagelok tube fitting and located in a 0.7 cm i.d. contraction, at about 5 cm upstream of the flow reactor. All experiments were performed at room temperature (T = 293 ± 3 K) and at ambient pressure using nitrogen (N_2) or synthetic air (N_2 and O_2) as the bath gas. Generally the volumetric flow rate was adjusted to 11 dm^3 min^{-1}, which resulted in about 19 s and

4 s residence times in the larger and smaller flow reactors, respectively. The gas flow velocities inside the flow tubes were varied in few of the experiments to inspect its possible effect on the ELVOC product distributions obtained. All experiments were performed under laminar flow conditions.

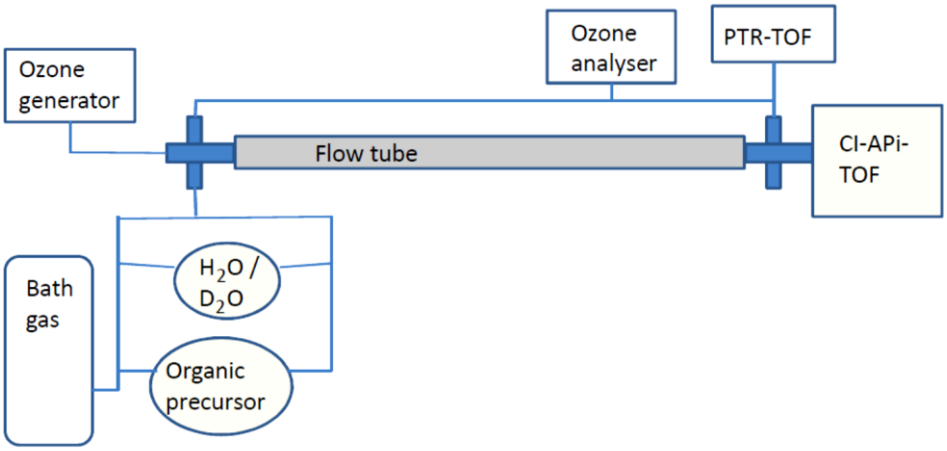

Figure S1 Simplified schematic of the experimental setup.

The concentration of cyclohexene in the gas flow was generally estimated from the vapor pressure of the precursor and the measured gas flows, but in some of the experiments the concentrations were directly determined using a PTR-TOF-MS (Proton Transfer Reaction Time-of-Flight Mass Spectrometer). The PTR-TOF-MS instrument consists of a proton transfer reaction (PTR) ion source and reaction chamber (Ionicon Analytik GmbH, Austria), where the VOCs of the sample air are ionized by hydronium ions (H_3O^+), and which is coupled to a time-of-light mass spectrometer (Tofwerk AG, Switzerland). A detailed description of the method can be found in[64, 65]. For the experiments, the PTR-TOF-MS was calibrated (see Taipale et al.[66] for details about the calibration set up) with a calibration gas mixture (Apel-Riemer Environmental Inc., USA) consisting of 16 different VOCs that was diluted with air purified by a catalytic converter. Ozone (O_3) concentration was measured concomitantly from the inflow and outflow of the flow reactor by an ozone analyzer (Thermo Scientific Model 49). Water (H_2O or D_2O) was added to the gas flow by bubbling a variable part of the bath gas flow through a water reservoir. The amount of water in the gas flow was not quantified further. The various types of experiments performed have been described in Table S1.

Table S1 Description of the experiments performed.

Reagent	**Reactor used**	**Volumetric flow, flow velocity, residence time / dm^3 min^{-1}, m s^{-1}, s**	**Bath gas**	**[a][O_3] range / 10^{12} molecule cm^{-3}**	**Added water; H_2O or D_2O**	**[Alkene] range / 10^{14} molecule cm^{-3}**
Cyclohexene	[b]long and short	11.4-15.6, 0.11-0.2, 4-19	Synthetic air, N_2	0.01-1.97	H_2O / D_2O	0.7-96.0
Cyclohexene d10	long	11.4-21.4, 0.11-0.2, 13-19	Synthetic air, N_2	0.01-1.97	H_2O / D_2O	0.44-14.7
cis-6-nonenal	long and short	5-11.5, 0.11-0.15, 4-19	Air, N_2	0.01-2.46	- / D_2O	0.05-3.6

[a]Concentration given by Thermo Scientific Model 49 Ozone Analyzer. [b]Long = 205 cm, 4.7 cm i.d. reactor; short = 63 cm, 4.0 i.d. reactor.

Experiments were conducted under increasingly oxidizing conditions that enabled studying the oxidation reactions further. During the experiments, more O_3 and organic precursor were added to the gas flow, which resulted in higher concentrations of radicals and intermediates in the mixture, and correspondingly higher probabilities for secondary reactions of the radicals formed. This was done in order to inspect the outcome of peroxy radical reactions (i.e., RO_2 + R´O_2, where R´= H or an alkyl-type group, possibly R = R´), and to reach conditions where the products of the RO_2 + RO_2 reaction can be seen with high enough signals for unambiguous identification.

S1.2. Chemicals

The chemicals cyclohexene (*c*-C_6H_{10}, 99.0%), deuterated cyclohexene (*c*-C_6D_{10}, 98%), *cis*-6-nonenal ($CH_3CH_2CH{=}CH(CH_2)_4CHO$, 92.0%) and deuterated water (D_2O, 99.9%) were obtained from the Aldrich chemical company. The water (H_2O) used was deionized and filtered with Millipore. The gases, nitrogen (N_2, cryogenic supply and 6.0 scientific grade, 99.999% and 99.9999%, respectively) and synthetic air (N_2 and O_2, 99.999%) were obtained from AGA. Ozone (O_3) was produced by a commercial ozone generator Dasibi 1008-PC, either from synthetic air or from pressurized and filtered air. All the chemicals were used without further purification.

S1.3. Uncertainties

It should be pointed out that the ELVOC yield determined here is very sensitive to the calibration factor used, and thus the CI-APi-TOF was calibrated with sulfuric acid (H_2SO_4) by producing a known amount of it from a reaction of SO_2 with OH-radicals, O_2 and H_2O (more on calibration below) [see ref.[91], and references therein]. However, the ion transmission efficiencies for ELVOCs and H_2SO_4 most likely differ, and thus

using a calibration coefficient determined for H_2SO_4 adds uncertainty to the values obtained. Other sources of uncertainty result mainly from calibration of mass flow controllers (i.e., gas flow rates and their calculations), ELVOC wall loss rate(-s), impurities in gas flows capable of reacting with the ELVOC precursors (e.g., HO_2 and RO_2 radicals produced from impurities) and uncertainties in determined O_3 concentrations. By adding the different uncertainties with a propagation of error method, one arrives at an estimated total uncertainty of the ELVOC yield of (4.5 ± 3.8)% for the C_6H_{10} + O_3 reaction (i.e., 80% estimated overall uncertainty; more on yield below).

S1.4. Water addition

We cannot detect individual H_2O (or D_2O) directly with the experimental setup, but we have an indirect proxy for the water abundance in the system; the $H_2O*NO_3^-$ complex (or equivalently $D_2O*NO_3^-$ when using D_2O). We found no evidence that indicates a role for water in the ELVOC formation. This is illustrated in Figure S2, where a few of the major ELVOC signals obtained are plotted together with the $H_2O*NO_3^-$ complex signal for one set of these experiments.

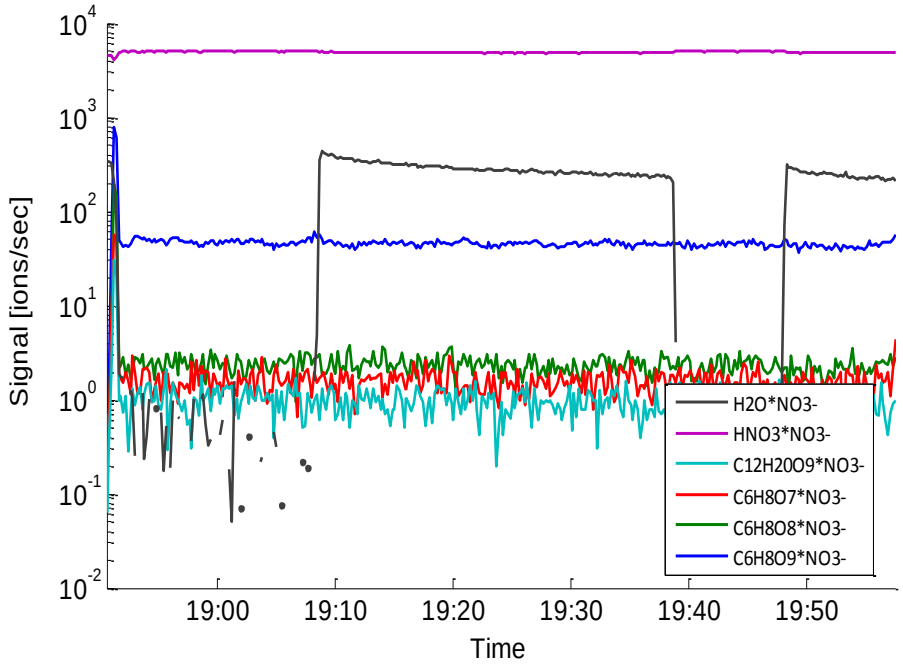

Figure S2 The identified ELVOC signals remain constant when H_2O is added to the gas flow. The addition can be seen from the sharp rise of the water-nitrate-ion complex signal ($H_2O*NO_3^-$) at 79.9989 Th. The ELVOC signals shown are: $C_6H_8O_9$, $C_6H_8O_8$ and $C_6H_8O_7$, detected as clusters with NO_3^- at 286.0052 Th, 270.0103 Th and 254.0154 Th, respectively.

By adding D_2O to the gas flow, instead of H_2O, we can get information on the chemical identity of the products formed, as acidic groups will exchange hydrogens easily[29, 85-87]. The deuterium atom is one mass

unit heavier than the hydrogen atom, and thus the identified ELVOC should shift one mass unit in the spectra for every exchangeable hydrogen atom in the ELVOC molecule. These investigations suggested that the product observed at 254.0154 Th ($C_6H_8O_7$) is formed through one O_2 addition step earlier intermediate than the 270.0103 Th and 286.0052 Th peaks (i.e., $C_6H_8O_8$ and $C_6H_8O_9$). This is because the 254.0154 Th peak was observed to shift only by two mass units, whereas the 270.0103 Th and 286.0052 Th peaks shifted by 3 mass units, indicating that 2 and 3 hydrogens were exchanged by D_2O addition to the reaction mixture, respectively (see Figures 1b and S3). This further suggests that the third hydroperoxide functionality is not yet formed in the 254.0154 Th's parent compound, the $C_6H_9O_8$ peroxy radical (see Scheme 2).

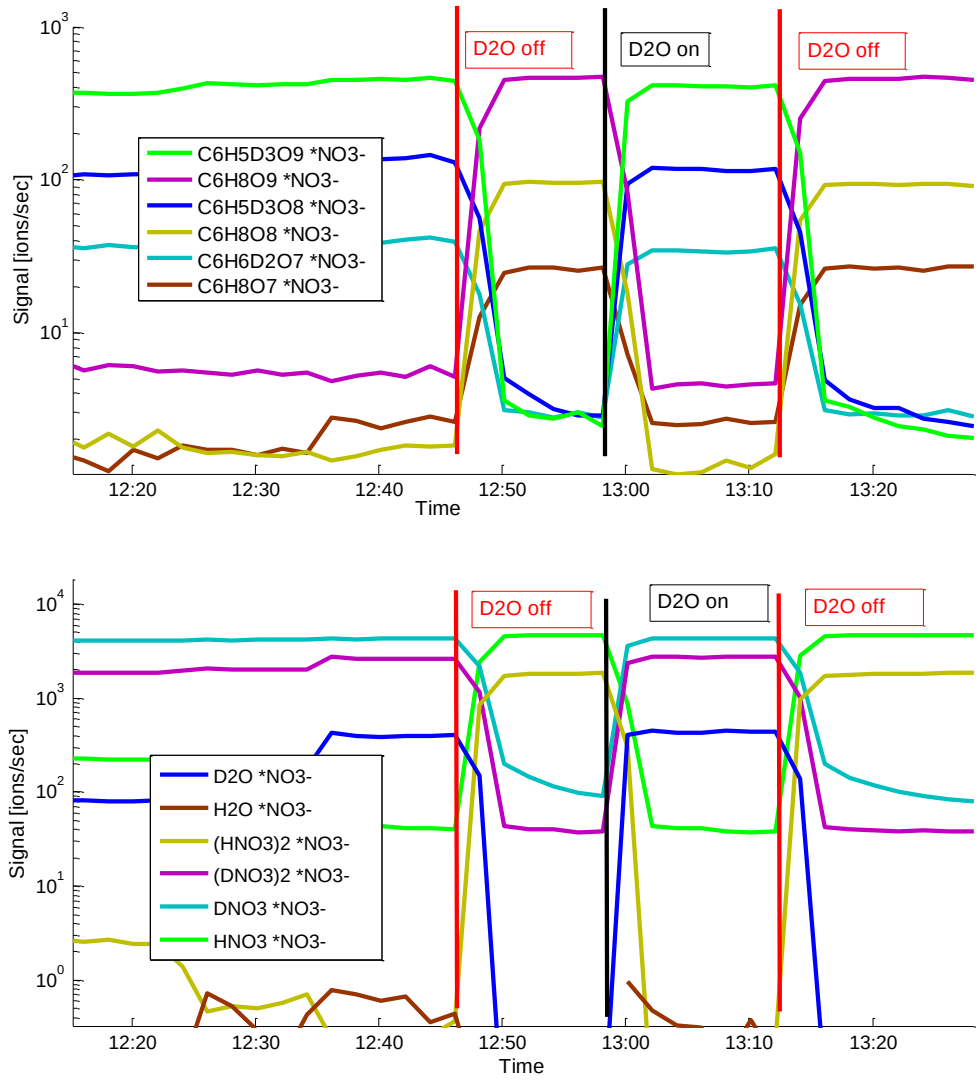

Figure S3 An example of how cyclohexene ozonolysis derived ELVOC signals shift in mass after adding D_2O to the gas flow (e.g., $C_6H_8O_9$ → $C_6H_5D_3O_9$). Also the charger nitrate clusters shift according to the amount of acidic hydrogens in the clusters.

S1.5. Deuterated cyclohexene, C_6D_{10}

The ELVOCs observed in the ozonolysis of deuterated cyclohexene were given in Table 1 and Figure 3, and the general monomer formation mechanism is believed to be analogous to the non-substituted cyclohexene ozonolysis system (see Scheme 2). By inspecting the mechanism and the peaks identified, it is observed that multiple D-atoms are exchanged to H-atoms before detection in both of the main products, i.e., the ELVOC product at 275.0417 Th is detected with a composition $C_6D_5H_3O_8$ (corresponding to $C_6H_8O_8$ in the C_6H_{10} + O_3 reaction) and the 293.0491 Th product is observed to have a composition $C_6D_7HO_9$ (corresponding to $C_6H_8O_9$ in the C_6H_{10} + O_3 reaction). In addition, the $C_6D_5H_3O_9$ at 291.0366 Th, the $C_6D_7HO_8$ at 277.0542 Th and the fully deuterated ELVOCs at 278.0605 Th ($C_6D_8O_8$) and 294.0554 Th ($C_6D_8O_9$) are seen but with reduced intensity.

By looking at the Figures 1a and 3a it is clear that the distribution of oxidation products has changed upon exchanging H-atoms with D-atoms in the cyclohexene precursor molecule. The deuterated ELVOC, $C_6D_8O_9$ (a major part of it is seen as $C_6D_7HO_9$ in the spectra at 293.0491 Th and less as $C_6D_5H_3O_9$ at 291.0366 Th), corresponding to the major monomer ELVOC detected in the C_6H_{10} + O_3 reaction (i.e., 286.0052 Th, $C_6H_8O_9$), is seen with much lower intensity (see Figures 1 and 3 for the spectra), as expected due to slower D-transfer reactions compared to H-transfer reactions, and also due to more probable tunneling for the lighter H-atoms[84]. In fact, the major monomer product observed in the C_6D_{10} + O_3 reaction is $C_6D_5O_8H_3$, detected at 275.0417 Th, and corresponding to the 270.0103 Th product of the C_6H_{10} + O_3 reaction ($C_6H_8O_8$); with three D-atoms exchanged prior to detection. Also, the product distribution has shifted toward the middle product due to hindered atom transfer of D in comparison with H.

S1.6. Dimers

When the O_3 and cyclohexene concentrations are increased enough, dimers appear in the spectra (Table 1, Figures 1 and 3). The dimers in this context are not dimers in the most conventional sense, that is, they're not formed by two similar pieces sticking together by Van der Waals forces and hydrogen bonds. Instead, they are distinctive species formed in the recombination and cross-combination reactions of different RO_2 radicals[12]. This can be seen from, for example, their elemental compositions, as the dimers have more than double the amount of hydrogens than the monomer species (i.e., they're not clusters of the same species).

In dimers the effect of OH-chemistry (which runs in parallel with ozonolysis, if no scavengers have been applied) is seen to interfere as we detect dimer compounds that apparently have not lost H-atoms during the oxidation sequence (e.g., $C_{12}H_{20}O_x$ species in Table 1). This indicates that there are some RO_2 species reacting which have more hydrogens than the original C_6H_{10} parent molecule, which is in contrast with

Scheme 2 where the first H-atom is lost in the prompt VHP decomposition. This can be explained by OH-chemistry, as the OH addition to the double bond of cyclohexene leads to a carbon-centered radical that has one H- and O-atom more than the unsaturated parent compound; cyclohexene (C_6H_{10}) will be converted to a carbon-centered hydroxycyclohexyl radical ($\bullet C_6H_{10}OH$) that adds an O_2 molecule and forms an oxygen-centered hydroxycyclohexyl peroxy radical ($\bullet O_2C_6H_{10}OH$; $C_6H_{11}O_3$). When these radicals react with the peroxy radical intermediates from Scheme 2, we obtain the dimer products with a carbon and hydrogen composition of $C_{12}H_{20}$ (see Figure 1 and Table 1).

Also another type of dimers in Table 1 might cause confusion at first - those with one less carbon atom in the elemental formula, i.e., C_{11}-compounds. As shown in the current and previous work[14, 17, 20], H-shifts leading to carbon-centered acyl-type radicals may lead to breakage of the carbon backbone by ejecting a CO-fragment. In cyclohexene ozonolysis, a C_5 carbon-centered alkyl-type radical is created concurrently (Scheme 2), which can add an O_2 molecule, forming a new C_5 peroxy radical, and react with the abundant C_6 peroxy radicals creating the C_{11}-dimers observed.

The $C_6H_{10} + O_3$ dimer deuteration experiments using D_2O mostly lead to two hydrogens being exchanged, but also to three and four hydrogen exchanges in the heaviest dimer products observed, consistent with the peroxide structures [i.e., ROOR or R(O)OO(O)R)] formed by recombination of two peroxy radicals containing hydroperoxide functionalities. Also the addition of D_2O to the $C_6D_{10} + O_3$ system provided valuable information: the deuterated dimers had exchanged their labile deuteriums to hydrogens prior to detection, but by adding D_2O to the bath gas flow these hydrogens were observed to exchange back to deuteriums. In this way it was found that the deuterated dimers contained one to three exchangeable hydrogens, which is less than what was observed for the $C_6H_{10} + O_3$ case.

The two most intense dimer peaks detected in the $C_6D_{10} + O_3$ reaction were $C_{12}D_{18}H_2O_7NO_3^-$ (356.2223 Th) and $C_{12}D_{16}H_2O_{10}NO_3^-$ (400.1788 Th) (Table 1). Note that the $C_{12}D_{18}H_2O_7NO_3^-$ product has altogether 20 H + D atoms and indicates interference by OH chemistry, as explained above. The deuterated dimers exchanged fewer hydrogens than the non-deuterated dimers, which is exactly what is expected when comparing reaction products that have been formed by hydrogen vs deuterium -shift reactions. Less hydroperoxide functionalities are effectively formed through the slower D-shift reactions. However, it is not certain that the NO_3^- will cluster in exactly the same way with the deuterated ELVOC as with the non-deuterated ELVOC molecules, although there is currently no reason to suspect otherwise.

It's also worth emphasizing that the dimers have on average higher H/C (or D/C) than the monomers, which indicates that their formation is in competition with the unimolecular termination pathways (i.e., ejecting OH and HO_2 radicals) forming the monomer compounds.

S1.7. *cis*-6-nonenal ozonolysis

Cis-6-nonenal ozonolysis produces a similar Criegee Intermediate as the cyclohexene ozonolysis (CI 1 in Scheme S1 and CI in Scheme 1, respectively), albeit with different internal excitation and lesser yield due to the concomitant formation of another type of three carbon Criegee Intermediate (CI 2 in scheme S1). The *cis*-6-nonenal ozonolysis was observed to lead to a similar monomer ELVOC distribution as the cyclohexene ozonolysis (Figure 1a and Figure 3c), consistent with the proposed formation mechanism.

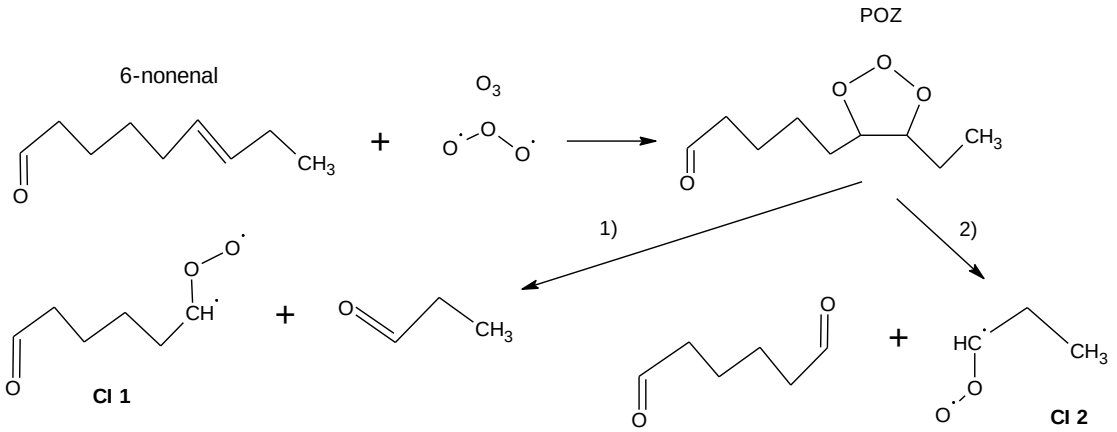

Scheme S1 *cis*-6-nonenal ozonolysis leads to two different Criegee intermediates CI 1 and CI 2, through O_3 addition, primary ozonide (POZ) formation and decomposition.

The nonenal ELVOC deuteration experiments did not yield a quantitative H/D exchange as can be seen in Figure S4. Most likely the residual H_2O in the system prevented from obtaining a complete H/D exchange. Another explanation could be the formation of isomers with different functional groups that are not able to exchange hydrogens. However, the charger nitrate ion distribution presented in Figure S4c, which experiences the same incomplete H/D exchange, indicates that there are still plenty labile H atoms in the system (probably due to residual H_2O) capable of exchanging D to H, and thus explains the observed product distribution.

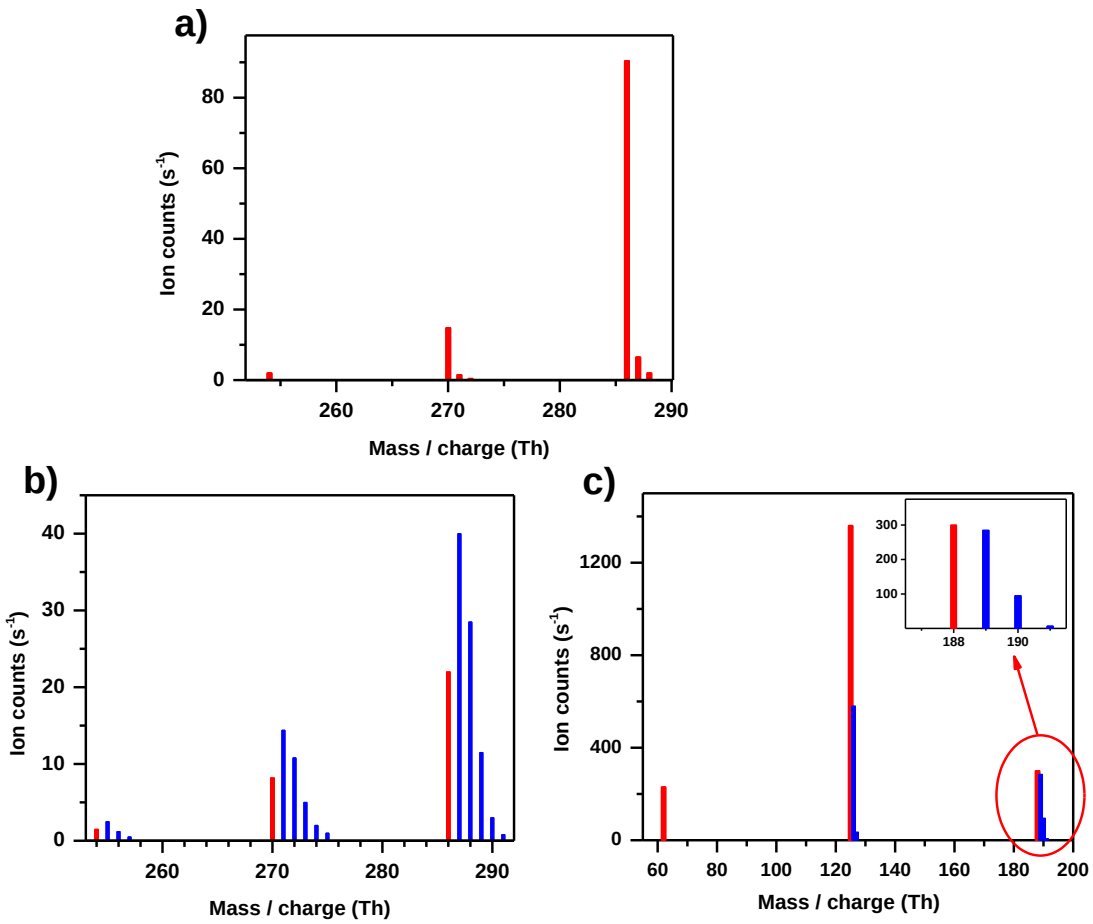

Figure S4a-S4c ELVOC spectra from *cis*-6-nonenal experiments. **a)** *cis*-6-nonenal ozonolysis ELVOC spectrum (Figure 3c in manuscript text) and **b)** the same nonenal ELVOCs after adding D_2O to the gas mixture. **c)** Charger nitrate ion clusters also exchange their acidic hydrogens, i.e., $HNO_3*NO_3^-$ → $DNO_3*NO_3^-$ and $(HNO_3)_2*NO_3^-$ → $HNO_3DNO_3*NO_3^-$, $(DNO_3)_2*NO_3^-$; the inset in the upper right corner shows the incomplete H/D-exchange of the nitrate trimer charger ion. Blue color indicates peaks with D atoms.

S1.8. ELVOC molar yield

The detection efficiency of the nitrate CI-APi-TOF to ELVOC was very recently estimated to be similar to the detection efficiency of H_2SO_4[12], and thus we used a calibration factor obtained for H_2SO_4 to convert the measured ion signals into concentrations. Hence, the CI-APi-TOF was calibrated by generating a known amount of H_2SO_4 from a SO_2 + OH (+ O_2 + H_2O) reaction[91]; OH-radicals were photochemically produced and the H_2SO_4 subsequently formed is readily measured by the nitrate CI-APi-TOF[62]. The calibration resulted in a factor of $C_{H2SO4} = 1.94 \times 10^{10}$ molecule cm^{-3}.

In addition to the calibration factor, one needs to take into account the amount of available charge carriers able to transfer the charge to the target species. In practice this was done by normalizing the product ion signals obtained by the amount of principal charge carriers {nitrate ion (NO_3^-) and its dimer ($HNO_3*NO_3^-$) and trimer [$(HNO_3)_2*NO_3^-$]} in the gas mixture. With these procedures one arrives at an equation (eq.S1) for individual ELVOC concentration:

$$[ELVOC] = C_{H2SO4} \times \frac{[ELVOCxNO_3^-]}{[NO_3^-]+[HNO_3NO_3^-]+[(HNO_3)2NO_3^-]} \quad \text{(eq.S1)}$$

The yield measurements were performed under pseudo-steady-state conditions, i.e., under conditions where the observed ELVOC signals remain effectively constant for as long as the experimental conditions remain unchanged in the flow reactor system, e.g., from several minutes to up to an hour in comparison with 4 to 20 s residence time in the flow tube (see Figure S2 and S3). This was accomplished by adjusting the reagent concentrations in the gas flow and letting the system relax into a balance where the observed rate of change of the gas composition was zero. For cyclohexene ELVOCs, under these conditions, the production term is equal to the cyclohexene ozonolysis rate {i.e., $k_{C6H10+O3} \times [O_3][CH]$, corrected by the ELVOC molar yield (Y_{ELVOC})} and the loss happens by wall reaction, but potentially also by other ways not easily separable from the experimental data. For practical purposes, the loss processes can be grouped under a common first-order loss rate (k_{LOSS}), provided the yield measurements are performed under conditions where the observed ELVOC yield is first-order with respect to the production term. The pseudo-steady-state can then be presented as:

$$d[ELVOC]/dt = k_{C6H10+O3} \times Y_{ELVOC} \times [O_3][CH] - k_{LOSS} \times [ELVOC] \approx 0 \quad \text{(eq.S2)}$$

As ELVOCs have by definition a very low vapor pressure, their wall losses in a flow tube are expected to be substantial. Fortunately, their extremely low vapor pressures also mean that no significant re-evaporation of the ELVOC is expected. In order to estimate the fraction of ELVOCs lost to the walls of the flow tube, a diffusion limited first-order wall loss rate ($k_{WALL} = 3.65\ D / r^2$, where r is the radius of the flow reactor) was calculated by applying a similar ELVOC diffusion constant as used by Ehn et al.[12] for α-pinene derived ELVOCs ($D = 0.05$ cm^2 s^{-1}). The normalized and calibrated ion counts obtained for the ELVOC were then corrected by the calculated wall loss fraction and the final yield determined with:

$$Y_{ELVOC} = (k_{LOSS} \times [ELVOC]) / (k_{C6H10+O3} \times [O_3][CH]) \quad \text{(eq.S3)}$$

where $k_{C6H10+O3} = 7.4 \times 10^{-17}$ cm^3 molecule^{-1} s^{-1} was taken from the most recent determination[33]. Only the peaks with identified elemental compositions were included in the ELVOC yield calculations (Table 1), and

hence, the quoted value is a lower limit for the ELVOC yield from cyclohexene ozonolysis system. Nevertheless, even by inspection of Figure 1a it's clear that these peaks contain most of the product ELVOCs and by omitting a part of the lower intensity peaks is not expected to lead to a large error, probably at most around 10% of the determined value.

The yield of ELVOCs is seen to increase together with the product of [cyclohexene] and [O_3] as expected[12] (Figure 4), and the yield determined for the C_6H_{10} + O_3 reaction system was (4.5 ± 0.2)%, with the uncertainty reported as one standard error of the fit. The overall uncertainty of this value was estimated as ±80%, and was obtained by the propagation of error method. It should be stressed that the yield determined in this work corresponds only to a few percent of the total product yield and does not seek to explain the formation of already well-established major products of the reaction given in previous publications[29-57].

S1.9. Relation to previous studies

Due to its structural similarity with the biogenic monoterpenes the cyclohexene ozonolysis system has attracted considerable attention. It has been a model system for deriving ozonolysis mechanisms and gaining insight into ambient SOA formation processes[33, 35, 49, 52-54]. The major products of the C_6H_{10} + O_3 reaction have been obtained previously, with various acids, diacids and oxo-acids identified in the gas- and particle phases, for example, adipic and glutaric acids have been frequently cited[33, 34, 49, 51, 52, 56, 57]. The OH-yield of cyclohexene + O_3 reaction has been determined most recently as 0.47[33] with only a small difference in the yield measured for the C_6D_{10} + O_3 reaction; OD yield of 0.50[29].

The role of radical chemistry in controlling the product distributions in cyclohexene SOA formation was emphasized by Keywood and co-workers[31]. They provided evidence on the role of acyl peroxy radical [i.e., •O-O-C(=O)-R] reactions, which had already previously been suggested to participate in SOA formation[31, 92]. In the current work, acyl peroxy radicals are seen to be important in ELVOC formation too (Scheme 2). However, acyl radical reactions (i.e., precursors for acyl peroxy radicals) lead to various different types of products as well, for example, they're known to be prone to dissociation by losing a CO fragment[20, 33, 88], which is the reason for C_{11}-compounds detected in the dimer product distribution (see discussion above). Acyl peroxy radical recombination, on the other hand, leads to diacyl peroxides, which Ziemann[32] suggested as important low volatility nucleating agents in the oxidation of cyclohexene. Nevertheless, the channels leading to ELVOCs have low yields[12], and only a small part of the produced acyl radicals will transform into ELVOCs. Müller et al.[55] found ester products as the possible oligomerizing, and hence, nucleating agents in cyclohexene ozonolysis, but concluded that other products could be contributing too.

Warren et al.[42] observed an increase in cyclohexene SOA yield under humid conditions and attributed this to an increase in aldehyde formation by a sCI + H_2O reaction. In this work, we see no influence of H_2O to the ELVOC spectrum obtained, and hence, this increase does not seem to result from ELVOCs reacting. In addition, Müller et al.[55] saw no relative humidity (RH) dependence on product formation. Moreover, according to the most recent previous studies[30, 36] the cyclohexene ozonolysis should not produce a stabilized Criegee intermediate and thus should not react appreciably with water in this system due to its very short lifetime. In a study by Carlsson et al.[33] it was observed that the presence of SO_2 in the cyclohexene ozonolysis gas mixture greatly enhanced particle formation through H_2SO_4 production and they pointed out that the SOA formation in the cyclohexene ozonolysis system is due to "chemical activation driven dynamics in the vinylhydroperoxide channel", which is exactly what is inferred from the results of this study too.

Tantamount to the mechanism proposed in this work is the formation of peroxy radicals (RO_2) by O_2 addition to the carbon centered radicals formed in the hydrogen shift step. While RO_2 radicals have not generally been observed to react with O_2, the carbon-centered alkyl radicals (R) will be converted to peroxy radicals ($R + O_2 \rightarrow RO_2$) practically instantly in ambient air. Alkyl radicals are known to react with a wide variety of species, while RO_2 mainly react with NO, HO_2 and RO_2 [82, 88]. Due to the RO_2 reacting with only a few species, the probability of RO_2 unimolecular reactions (isomerization and fragmentation) significantly increases[93], especially under pristine atmospheric conditions where [NO] is low.

The arguments previously found to hold for 1,x hydrogen shifts seem to be valid for the ELVOC formation too, e.g., close-by oxygenated functional groups catalyze the process but abstraction from the neighboring carbon atom is generally forbidden due to high ring strain in the transition state[17, 19, 94, 95]. Thus the hydrogen abstractions will most likely occur in places where the hydrogens are weaker bonded due to the electron withdrawing inductive effects of properly situated functional groups. For example, oxygenated groups such as hydroperoxy, carbonyl or hydroxyl in the α-carbon have been observed to lower the H-abstraction barriers significantly[19, 94]. In line with this, the aldehydic hydrogens (i.e., H-atoms in terminal -CHO groups) are generally rather weakly bound and often the easiest to abstract. It is these relatively weak C-H bonds that facilitate the peroxy radical isomerization to a hydroperoxide (commonly noted: $RO_2 \rightarrow QOOH$) even at room temperature; a reaction class extensively investigated in combustion[14, 96]. However, the RO_2 isomerization is also in competition with a route leading to HO_2 elimination, and the HO_2 yield has been observed to increase and shift to lower temperatures when the carbon skeleton lengthens[16, 88].

Ultimately, the formation of ELVOC from cyclohexene seems to be governed by the amount of abstractable hydrogen atoms in the carbon skeleton, which are loosened from the backbone by the presence of nearby oxygenated functional groups. The proposed chain like mechanism starting from ozonolysis leads to the generation of an additional OH-radical on top of the VHP decomposition, and may thus explain, in part,

some of the discrepancy observed in the heightened OH-levels over specific forested environments dominated by biogenic emissions[94, 97, 98]. The proposed mechanism offers another type of explanation without invoking the recycling mechanisms[94, 98-101], which likely run in parallel to the reaction sequences described in the current paper. The mechanism presented here is strictly valid only for cyclohexene ozonolysis, but similar reaction sequences can be expected to happen in different alkene ozonolysis reactions. For example, in monoterpene oxidation by O_3 for which $C_6H_{10} + O_3$ can be considered a surrogate reaction.

S2. Quantum chemical calculations

S2.1. Validation of configurational sampling algorithm

For the 1,7 hydrogen shift and CO loss reactions of $C_6H_9O_4$, the ROHF-RCCSD(T)-F12a/VDZ-F12 energy was calculated for every reactant, transition state (TS) and product conformer (over 100 conformers in total) in order to test the validity of the sampling method. While the absolute reaction energetics (e.g., energy difference between transition states and reactants, or reactants and products) predicted by the different methods differed significantly (by several kcal/mol), the relative energies of different conformers of the same system (i.e., different torsional conformers of the same reactant, TS or product) were close to each other. The relative energy is here defined as the energy of a conformer minus that of the lowest-energy conformer of the same type (reactant, TS or product).

The average unsigned difference between the ωB97XD/aug-cc-pVTZ and ROHF-RCCSD(T)-F12a/VDZ-F12 relative energies were 0.24, 0.44, 0.08 and 0.08 kcal/mol for the reactants, H-shift transition states, products and CO loss transition states, respectively. The largest difference observed was 0.80 kcal/mol, for one of the H-shift transition states. Even more encouragingly, despite the total number of conformers exceeding 100, both methods predicted the same conformer to have the lowest energy for all four systems (reactant, product and two transition states).

Also the B3LYP/6-31+G(d) relative energies (of the B3LYP-optimized structures) were surprisingly close to the final ROHF-RCCSD(T)-F12a/VDZ-F12 values, with average unsigned differences of 0.39, 0.58, 0.74 and 0.20 kcal/mol for the reactants, H-shift transition states, products and CO loss transition states, respectively. The largest difference observed between B3LYP and CCSD(T) relative electronic energies was 1.55 kcal/mol, for one of the reactant structures. This suggests that picking the structures within 2 kcal/mol of the minimum at the B3LYP/6-31+G(d) level for further calculations is a reasonable strategy for finding the global minimum-energy structure at the ROHF-RCCSD(T)-F12a/VDZ-F12//ωB97XD/aug-cc-pVTZ level.

S2.2. TST versus MC-TST

Table S2 shows the partition functions obtained using only the lowest-energy conformer, or all the conformers included. Table S3 shows the rate coefficients obtained using only the lowest-energy conformers (as in conventional TST), and using MC-TST.

Table S2 The partition functions of the reactants, transition states and products for each reaction.

	Lowest-energy conformer [a]				**Including all conformers** [b]		
Label	Q_R	Q_{TS}	Q_P		Q_R	Q_{TS}	Q_P
$C_6H_9O_4$ 1,7 H-shift	1.4×10^{10}	4.5×10^{8}	1.7×10^{9}		1.6×10^{11}	1.2×10^{9}	6.5×10^{10}
$C_6H_9O_4$ CO loss	1.7×10^{9}	1.6×10^{10}	-		6.5×10^{10}	1.5×10^{11}	-
$C_6H_9O_6$ 1,8 H-shift	2.6×10^{10}	4.1×10^{9}	2.1×10^{11}		2.6×10^{10}	9.5×10^{9}	3.1×10^{12}
$C_6H_9O_6$ 1,7 H-shift	2.6×10^{10}	2.7×10^{9}	9.9×10^{10}		2.6×10^{11}	7.0×10^{9}	1.5×10^{11}
$C_6H_9O_6$ CO loss	2.1×10^{11}	7.8×10^{10}	-		3.1×10^{12}	1.5×10^{13}	-
$C_6H_9O_8$ 1,7 H-shift	2.3×10^{12}	1.5×10^{11}	2.6×10^{12}		5.4×10^{13}	1.9×10^{11}	4.6×10^{13}
$C_6H_9O_8$ 1,4 H-shift	2.3×10^{12}	5.9×10^{11}	-		5.4×10^{13}	2.5×10^{13}	-
$C_6H_9O_8$ 1,5 H-shift	2.3×10^{12}	6.4×10^{11}	-		5.4×10^{13}	1.1×10^{12}	-
$C_6H_9O_8$ 1,6 H-shift	2.3×10^{12}	4.8×10^{11}	4.4×10^{11}		5.4×10^{13}	1.4×10^{12}	3.9×10^{13}

[a]The partition function of the lowest energy conformer (Q), and, [b]the partition function using all conformers of the reactant (R), transition state (TS) and product (P) for each reaction. The partition function is a product of the rotational and vibrational partition function. The ratios of Q_{elec} and Q_{trans} are assumed to be equal to 1 for all reaction steps studied here, and therefore cancel out in the rate coefficient calculations. Note that the reactant of the CO loss reaction is the same as the product of one of the H-shift reactions.

Table S3 Calculated rate coefficients for the different H-shift and CO loss reactions.

	Barriers (kcal/mol)		k_{TST} (s^{-1}) [a]		k_{MCTST} (s^{-1}) [a]		
Reaction	**Forward**	**Reverse**	**Forward**	**Reverse**	**Forward**	**Reverse**	**κ (tunneling)**
$C_6H_9O_4$ 1,7 H-shift	15.6	14.7	7.9×10^{-1}	29	1.7×10^{-1}	2.0	44
$C_6D_9O_4$ 1,7 D-shift	16.3	15.7	1.9×10^{-1}	4.4	-	-	6.4
$C_6H_9O_4$ CO loss	14.2		2.2×10^{3}	-	5.1×10^{2}	-	-
$C_6H_9O_6$ 1,8 H-shift	18.0	24.2	6.5×10^{-2}	2.4×10^{-7}	1.5×10^{-2}	3.8×10^{-8}	33
$C_6D_9O_6$ 1,8 D-shift	18.7	25.2	1.6×10^{-2}	3.8×10^{-8}	-	-	5.1
$C_6H_9O_6$ 1,7 H-shift	16.7	29.8	3.7×10^{-1}	2.3×10^{-11}	9.7×10^{-2}	4.0×10^{-11}	39
$C_6H_9O_6$ CO loss	9.5		2.4×10^{5}	-	3.3×10^{6}	-	-
$C_6H_9O_8$ 1,7 H-shift	19.9	22.8	1.2×10^{-3}	7.1×10^{-6}	6.2×10^{-5}	5.2×10^{-7}	723
$C_6D_9O_8$ 1,7 D-shift	21.0	23.8	1.5×10^{-4}	1.1×10^{-6}	-	-	22
$C_6H_9O_8$ 1,4 H-shift	22.4	-	6.5×10^{-5}	-	1.1×10^{-4}	-	≈10 [b]
$C_6H_9O_8$ 1,5 H-shift	21.0	-	7.6×10^{-4}	-	5.7×10^{-5}	-	-
$C_6H_9O_8$ 1,6 H-shift	19.8	18.4	4.2×10^{-3}	2.2×10^{-1}	5.2×10^{-4}	7.1×10^{-3}	200

[a]Note that rates do not include tunneling corrections. [b]The exact Eckart tunneling factor could not be completed due to the lack of data on the reverse barrier; test calculations varying the reverse barrier in a wide range between 10 and 50 kcal/mol indicate that the tunneling factor is very likely between 8 and 12.

S2.3.1 Assessing the effect of hindered rotors: uncoupled models

We evaluated the effect of hindered rotations on the rate coefficients using the hindered rotor module of the Gaussian 09 program suite[77-80]. Specifically, we ran a hindered rotor frequency calculation for all the reactants, transition states and products with the lowest zero-point corrected energy. However, for many of these structures, the program was unable to find a one-to-one correspondence between vibrational and internal rotation modes, and thus did not calculate hindered rotor-corrected partition functions, energies, entropies or other thermodynamic parameters. Closer inspection revealed that the problem occurred for all transition states, and also for some (though not all) of the reactants and products containing internal hydrogen bonds, which may partially constrain the internal rotations.

In order to qualitatively assess the effect of hindered rotations on the reaction energetics, we did the following. For the reactants and products for which the hindered rotor module worked on the lowest-energy conformer (specifically, the $C_6H_9O_4$ reactant and product and the $C_6H_9O_6$ product), we used the values from those calculations. For the $C_6H_9O_6$ reactant and the $C_6H_9O_8$ 1,7 H-shift reactant and product (for which the hindered rotor module failed), we constructed a new set of conformers, where the six carbon atoms were arranged linearly (i.e., the carbon chain did not loop back on itself), and the OOH groups were oriented so that no ring structures with hydrogen bonds could form. These conformers were naturally higher in energy than the respective minimum-energy conformers, and were only used for assessing the effect of internal rotations. For these systems, the hindered rotor module was able to calculate the desired corrections to thermodynamic parameters. Altogether, this resulted in a set of 49 identified hindered rotation modes (from the six studied molecules), for which average thermodynamic parameters could then be calculated.

The main effect of hindered rotations on the thermodynamic parameters is to increase the entropy, and thereby decrease the free energy. Hindered rotations also have a small effect on the thermal energy (including zero-point energy corrections), but this is not systematic – the energy can both increase and decrease. According to the results of the hindered rotor module, each hindered rotation increases the entropy by between about 0.06 and 0.46 cal/K mol, with an average value of 0.28 cal/K mol, and changes the thermal energy by between −0.05 and +0.064 kcal/mol, with an average value of +0.033 kcal/mol. These together change the Gibbs free energy (at 298.15 K) by -0.05 kcal/mol per torsional mode. These values correspond to the McClurg treatments; the model by Pitzer & Gwinn yields essentially identical results while that by Truhlar consistently predicts smaller effects. We used these average values to qualitatively assess the effect of hindered rotations on the rate coefficients. It should be noted that the Gaussian program also reports an entropic effect from the so-called ”multiplicity” of the hindered rotations, i.e., the fact that some internal rotations connect multiple accessible minima. This effect is already accounted for via the conformational sampling in the MC-TST rate coefficients (see section S2.2.), and is therefore not included in this calculation.

Since the products of hydrogen shift reactions have one more torsional angle than the reactants (due to the new OOH group), accounting for hindered rotations thus slightly increases the thermodynamic favorability of the hydrogen shift reactions (an entropy difference of 0.28 cal/K mol corresponds to an increase in the equilibrium constant of about 15 percent at 298 K). The increase in thermal energy acts in the opposite direction, but the magnitude of this effect is less than half of the entropic effect; about 6 percent. Compared to the other error sources in our calculations, the hindered rotor effect on the equilibrium constants is thus negligible.

Due to the constraints imposed by the reacting C-H…O-O groups, the hydrogen shift transition states have a smaller number of internal rotation degrees of freedom than the reactants and products. The net effect of the internal rotations is thus to lower both the forward and reverse rate coefficients. The magnitude of this effect depends on both the number of internal rotations in the reactants/products, and on the number of rotations constrained by the transition state. For the 1,7 H-shift transition state of $C_6H_9O_4$, and the 1,8 H-shift transition state of $C_6H_9O_6$, all but one of the internal rotations are constrained (see Figs S5 and S6). As discussed above, the combined entropic and energetic effects imply that one hindered rotation mode present in the reactant but not the transition state decreases the forward rate coefficient by approximately a factor of 1.09. Thus, the 1,7 H-shift of $C_6H_9O_4$ and the 1,8 H-shift of $C_6H_9O_6$ are slowed down by factors of about 1.5 and 1.7, respectively. The 1,7 H-shift transition state of $C_6H_9O_6$ (leading to OH loss) has one more internal rotation degree of freedom compared to the competing 1,8 H-shift transition state. This implies that the relative rate coefficient of the 1,7 H-shift will be further increased by a factor of 1.09 due to internal rotor effects. This does not change the qualitative conclusion that the branching ratios of the 1,7 and 1,8 H-shift channels are roughly 90% and 10%, respectively.

For the H-shift transition states of $C_6H_9O_8$, the number of internal rotations is 8, 7, 6 and 5 for the 1,4, 1,5, 1,6 and 1,7 H-shifts, respectively, compared to 10 for the reactant. This corresponds to decreases in the forward rate coefficient ranging from a factor of 1.2 (for the 1,4 H-shift) to 1.5 (for the 1,8 H-shift). The change in relative rates does not change the conclusion that the 1,6 and 1,7 H-shifts form the main channels for the $C_6H_9O_8$ radical.

The CO loss transition states have an equal number of internal rotations compared to their reactants, and the internal rotation corrections therefore largely cancel out.

S2.3.2 Assessing the effect of hindered rotors: MS-T modeling

Since many of the torsional modes of our molecules are likely strongly coupled to each other, the 1-dimensional torsional anharmonicity treatment implemented in the Gaussian Hindered Rotor module is likely

insufficient to fully model the effect of hindered rotations on the hydrogen shift reactions. Therefore, we performed further calculations using the MS-Tor program[80, 81], which is based on the multistructural approximation with torsional anharmonicity (MS-T)[102, 103]. The MS-Tor program is not designed to accept input structures with more than 7 torsional angles, preventing its direct application to our second hydrogen shift step $C_6H_9O_6$ (where the reactant has 8 torsional angles).

We treated the first hydrogen shift step (step 1a in Scheme 2) following the MS-Tor manual. We obtained a value of +1.1 kcal/mol for the effect of torsional anharmonicity on the free energy difference between the transition state and reactant at 298.15 K, calculated as the difference between the MS-LH ("multistructural local harmonic") and MS-T free energy values given by the MS-Tor program. This net effect was composed of enthalpy and entropy changes for both the transition state and the reactant. For the $C_6H_9O_4$ reactant, including all six torsions, going from MS-LH to MS-T increased the enthalpy (H) by 0.15 kcal/mol, and decreased the entropy contribution to the free energy (-TS) by -0.03 kcal/mol. In comparison, the simple uncoupled averaged approach described in section 2.3.1 predicted an enthalpy increase of 0.18 kcal/mol and a decrease in the entropy contribution of -0.48 kcal/mol, assuming six torsions in the reactant. For the transition state with one torsion, MS-Tor predicted an enthalpy decrease of -0.45 kcal/mol, and an increase in the entropy contribution (-TS) of +1.64 kcal/mol. It is surprising that the effect predicted for the transition state is so much larger than that for the reactant, as the former has only one (non-constrained) torsional degree of freedom, while the latter has six – one of which corresponds to exactly the same rotating group as in the transition state (the terminal CHO group). Closer inspection of the MS-Tor output indicates that its treatment of the transition states may be problematic for our system. For several conformers of the $C_6H_9O_4$ transition state, MS-Tor reported effective torsional barriers of less than 0.01 kcal/mol. In the corresponding reactant structures, the lowest torsional barriers were always above 1 kcal/mol, and usually at least 2 kcal/mol, even for the same rotating group (i.e. the terminal CHO group). Thus, while the MS-T model is considerably more advanced than the uncoupled model used in Gaussian's Hindered Rotor package, even the MS-Tor results must be considered qualitative for this particular system.

By modifying the program code, we were able to run MS-Tor also for $C_6H_9O_6$, but not $C_6H_9O_8$ (which has 10 torsional angles in the reactant). Treating the $C_6H_9O_6$ reactant required first modifying the program code to accept eight torsional modes as input, running MS-Tor to identify the effective torsional barriers, and then removing one of the torsions as its barrier was too high, leading to non-numerical ("NaN") output values for the MS-T thermodynamic parameters. After these modifications, we finally obtained a value of +0.5 kcal/mol for the effect of torsional anharmonicity on the free energy barrier of the 1,8 H-shift of $C_6H_9O_6$ (reaction 3a in Scheme 2). Closer inspection of the output revealed that the $C_6H_9O_6$ transition state (with 2 torsions) also had very low (< 0.01 kcal/mol) effective torsional barriers for many conformers.

The MS-Tor results indicate that torsional anharmonicity slows down the first H-shift step by a factor of 6, and the second by a factor of 2. The effect is thus somewhat larger than predicted by the 1-dimensional treatment in the Gaussian 09 program, but still fairly small compared to e.g. tunneling.

S2.4. Molecular structures and thermodynamic parameters of the studied system

Figures S5, S6 and S7 show the lowest-energy structures (at the ROHF-RCCSD(T)-F12a/VDZ-F12//ωB97XD/aug-cc-pVTZ level including zero-point energy corrections) for the $C_6H_9O_4$, $C_6H_9O_6$ and $C_6H_9O_8$ systems, respectively. The corresponding thermodynamic parameters are given in Table S4, and the cartesian co-ordinates in Table S5.

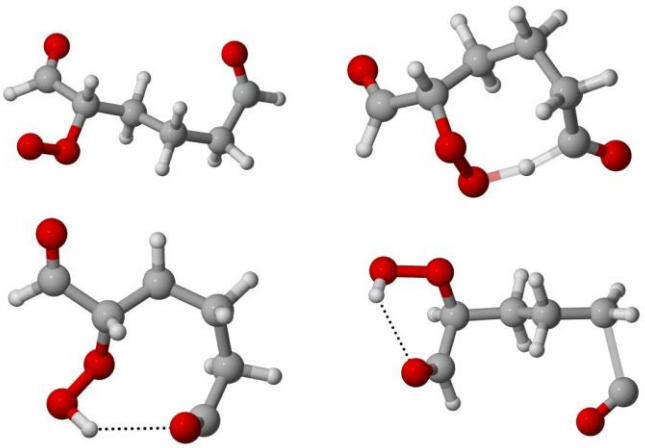

Figure S5 Lowest-energy structures for $C_6H_9O_4$. Top left: reactant. Top right: 1,7 H-shift transition state. Bottom left: product. Bottom right: CO loss transition state. Color coding: gray=carbon, red=oxygen, white=hydrogen.

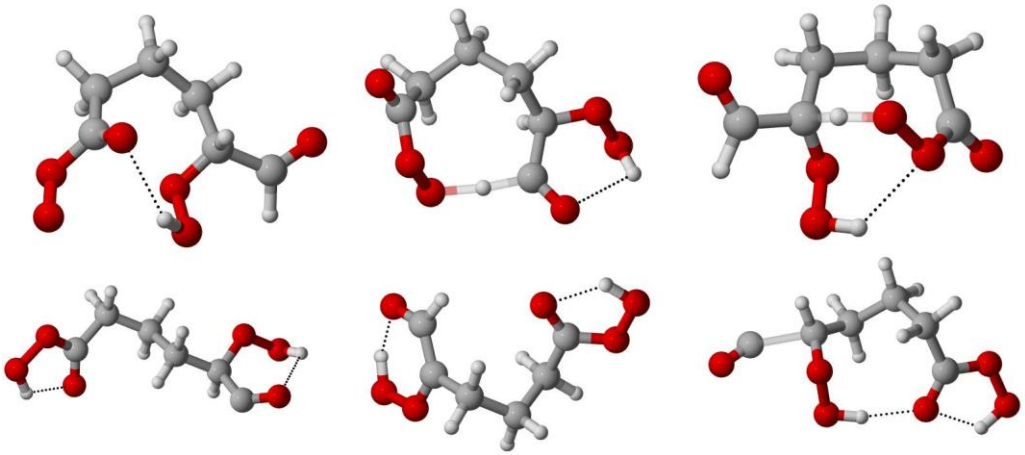

Figure S6 Lowest-energy structures for $C_6H_9O_6$. Top left: reactant. Top middle: 1,8 H-shift transition state. Top right: 1,7 H-shift transition state. Bottom left: 1,8 H-shift product. Bottom middle: 1,7 H-shift product. Bottom right: CO loss transition state. Color coding as in Figure S5.

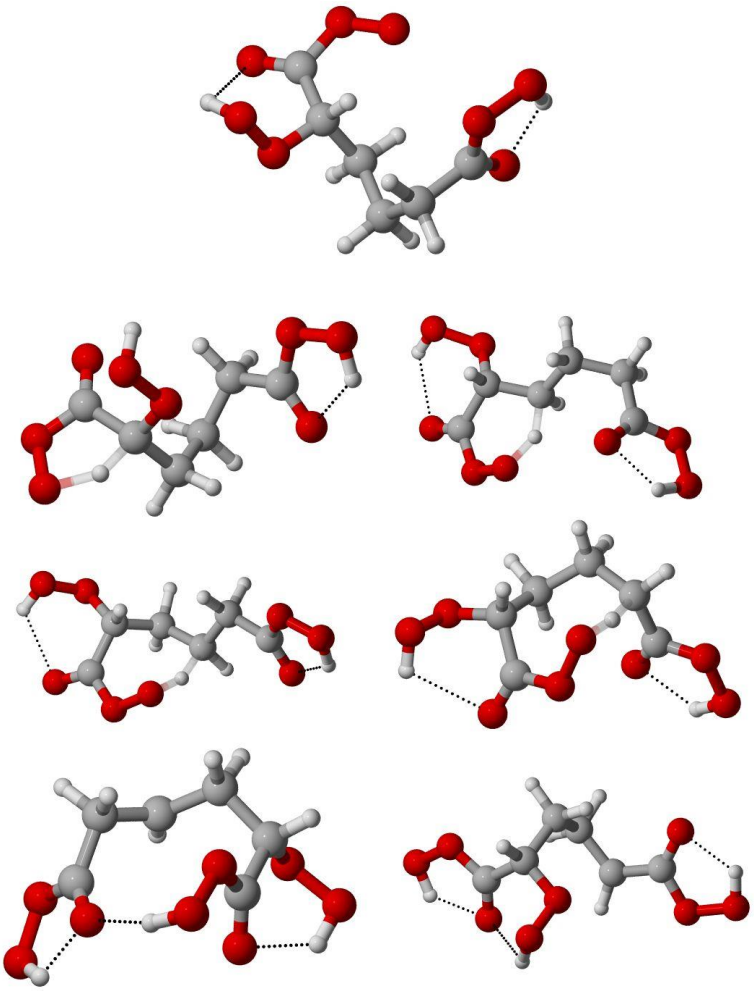

Figure S7 Lowest-energy structures for $C_6H_9O_8$. Top row: reactant. Second row left: 1,4 H-shift transition state. Second row right: 1,5 H-shift transition state. Third row left: 1,6 H-shift transition state. Third row right: 1,7 H-shift transition state. Fourth row left: 1,6 H-shift product. Fourth row right: 1,7 H-shift product. Color coding as in Figure S5.

Table S4 Energies, zero-point vibrational energies, thermal enthalpy and thermal free energy contributions of the structures shown in Figures S5-S7, and wavenumbers of the imaginary vibrational modes of the transition states.

name	**E_{elec}, DFT** [a, b]	**E_{elec}, F12** [a, c]	**ZPE, DFT** [d]	**H_{therm}** [e]	**G_{therm}** [f]	**Imag. mode** [g]
O_2	-150.33429845	-150.17736641	0.003881	0.007188	-0.016069	-
$C_6H_9O_4$ reactant	-534.824880717	-534.15339617	0.147996	0.160132	0.108268	-
$C_6H_9O_4$ 1,7 TS [h]	-534.798589759	-534.12466692	0.144093	0.154920	0.107580	1647.5i
$C_6H_9O_4$ 1,7 product [i]	-534.818448473	-534.15265521	0.148700	0.160676	0.110943	-
$C_6H_9O_4$ CO loss TS	-534.788765728	-534.12543581	0.144180	0.156836	0.104288	324.7i
$C_6H_9O_6$ reactant	-685.210047983	-684.39158629	0.157809	0.171450	0.117191	-
$C_6H_9O_6$ 1,8 TS	-685.184014815	-684.35868956	0.153573	0.166247	0.114695	1522.6i
$C_6H_9O_6$ 1,7 TS	-685.183123412	-684.36021210	0.153053	0.165806	0.114568	1552.1i
$C_6H_9O_6$1,7 product	-685.235734867	-684.41402811	0.159310	0.172617	0.117435	-
$C_6H_9O_6$ 1,8 product	-685.216831503	-684.40194656	0.158345	0.172347	0.115741	-
$C_6H_9O_6$ CO loss TS	-685.199920390	-684.38435707	0.155923	0.169908	0.114266	304.0i
$C_6H_9O_8$ reactant	-835.603426981	-834.63563540	0.167668	0.183337	0.122589	-
$C_6H_9O_8$ 1,4 TS	-835.566677026	-834.59460527	0.162282	0.177683	0.118478	1303.2i
$C_6H_9O_8$ 1,5 TS	-835.563800893	-834.59600828	0.161437	0.176412	0.117553	1827.8i
$C_6H_9O_8$ 1,6 TS	-835.566270440	-834.59777991	0.161327	0.176304	0.117723	1812.8i
$C_6H_9O_8$ 1,7 TS	-835.567518408	-834.59802378	0.161699	0.176439	0.119177	1938.3i
$C_6H_9O_8$ 1,6 product	-835.596984075	-834.63227092	0.166466	0.182142	0.122948	-
$C_6H_9O_8$ 1,7 product	-835.605611663	-834.63944183	0.166804	0.182701	0.121594	-

[a]Energies (with [b]DFT referring to ωB97XD/aug-cc-pVTZ, and [c]F12 referring to ROHF-RCCSD(T)-F12a/VDZ-F12), [d]zero-point vibrational energies, [e]thermal enthalpy, and, [f]thermal free energy contributions of the structures shown in Figures S5-S7, given in Hartree, at 298.15 K and 1 atm reference pressure. [g]Wavenumbers given in cm^{-1}. [h]"1,X TS", and, [i] "1,X product" refer to transition states and products of 1,X hydrogen shifts, respectively.

Table S5 Cartesian co-ordinates (in Ångström) of the structures shown in Figures S5-S7 and given in Table S4.

O_2 (triplet)

O	0.0	0.0	0.597986
O	0.0	0.0	-0.597986

$C_6H_9O_4$ reactant

C	-2.5739518	1.2524534	-0.3228367
H	-3.6006238	0.9247124	-0.5697497
C	-1.6652128	0.1555354	0.2187893
H	-1.6606948	0.2329174	1.3091033
C	-0.2614618	0.2005084	-0.3444957
H	0.1040662	1.2156884	-0.1933407
H	-0.3076148	0.0310974	-1.4234897
C	0.6764472	-0.8084966	0.3115523
H	0.2965712	-1.8184886	0.1574583
H	0.6971102	-0.6322566	1.3886893
C	2.0947262	-0.7237726	-0.2310237
H	2.1121462	-0.7492086	-1.3257187
C	2.8675442	0.4906404	0.2082923
H	3.8753802	0.5895794	-0.2414767
O	2.4728512	1.3066254	0.9957223
O	-2.2141578	2.3846354	-0.4574207
H	2.6886052	-1.5893366	0.0809223
O	-2.2489098	-1.1263556	-0.1103237
O	-3.3528198	-1.3364786	0.5493473

$C_6H_9O_4$ 1,7 H-shift TS

C	-2.3773989	-0.7902039	-1.0177839
H	-2.6907109	-1.8130539	-0.7390539
C	-1.3961369	-0.1451449	-0.0471519
H	-1.9676989	0.5522031	0.5746321
C	-0.2873569	0.5993891	-0.7800459
H	-0.7824159	1.3044401	-1.4474039
H	0.2406201	-0.1028799	-1.4270559
C	0.7003831	1.3600241	0.1047081
H	0.1726571	2.1296741	0.6705001

H	1.3987881	1.8791831	-0.5523109
C	1.5151351	0.5191751	1.1054181
H	0.8912851	0.2430691	1.9552321
C	2.0033581	-0.7707879	0.4904741
H	1.0118101	-1.5571679	0.3096961
O	3.1044801	-1.0784389	0.1935241
O	-2.7993019	-0.2350519	-1.9916789
H	2.3799451	1.0767491	1.4631011
O	-0.9455549	-1.1141029	0.8899301
O	-0.1718869	-2.0570739	0.2452691

$C_6H_9O_4$ 1,7 H-shift product

C	-2.5784244	0.2565130	0.1240697
H	-3.1698764	-0.4060090	-0.5345123
C	-1.0899994	-0.0541120	0.1742527
H	-0.8518874	-0.3965120	1.1870457
C	-0.2390604	1.1617490	-0.1670713
H	-0.6916984	2.0119660	0.3433227
H	-0.3194754	1.3550800	-1.2400773
C	1.2282116	1.0595690	0.2436927
H	1.2981346	0.8841590	1.3187707
H	1.6947416	2.0274080	0.0545367
C	2.0509366	0.0004770	-0.4973253
H	3.1209376	0.2111940	-0.4150883
C	1.9171126	-1.4140380	0.0033577
O	1.4509686	-1.8199680	1.0090997
O	-3.0797654	1.1526360	0.7428147
H	1.8307156	-0.0137070	-1.5650393
O	-0.7714094	-1.0735800	-0.7573373
O	-1.2813454	-2.3012370	-0.2570243
H	-0.5188164	-2.6415880	0.2325117

$C_6H_9O_4$ CO loss TS

C	3.3979236	-0.4450339	0.0378843
C	2.0723866	1.2382751	0.6191043
C	0.6970506	0.6697771	0.6567573
C	0.1165606	0.4200131	-0.7337137
C	-1.2695084	-0.2174029	-0.7162177
O	-2.1355014	0.6643301	-0.0500537

O	-3.4639884	0.1775541	-0.1835207
O	2.8714046	-1.4548809	0.0637853
C	-1.2276194	-1.5851669	-0.0649657
O	-1.8987054	-1.9056589	0.8780203
H	2.5715236	1.4310421	1.5597833
H	2.3356446	1.9153041	-0.1840567
H	0.0397076	1.3551121	1.2029723
H	0.6973436	-0.2556359	1.2411583
H	0.0502396	1.3588601	-1.2845037
H	-0.5208974	-2.2988409	-0.5325137
H	-1.6109984	-0.3690839	-1.7490187
H	0.7775966	-0.2367469	-1.3026027
H	-3.5001634	-0.4618169	0.5417023

$C_6H_9O_6$ reactant

C	1.9470966	0.0508505	-0.1259375
C	1.3627836	1.2933705	0.4671175
H	2.1170236	2.0738415	0.3328765
H	1.2531706	1.1468665	1.5412505
C	0.0468236	1.7188865	-0.1816425
H	0.1595626	1.7066495	-1.2667835
H	-0.1388684	2.7547175	0.1020835
C	-1.1757174	0.8946795	0.2200265
H	-2.0684364	1.3595895	-0.1980795
H	-0.8493114	-0.5818065	-1.3148265
H	-1.2953324	0.8974955	1.3066635
O	2.7679796	-0.5819635	0.8538225
O	3.2635586	-1.7209535	0.4541375
O	1.8447866	-0.3813875	-1.2241115
C	-1.1711084	-0.5479985	-0.2686385
C	-2.5495904	-1.1858305	-0.1817335
H	-2.5867984	-2.1407595	0.3737795
O	-3.5267554	-0.6939785	-0.6715915
O	-0.2481574	-1.2707975	0.5308475
O	0.0265556	-2.5038275	-0.1178515
H	0.8207356	-2.2876435	-0.6314095

$C_6H_9O_6$ 1,8 H-shift TS

C	0.3029300	-1.9228668	1.5033120

C	0.6197360	-0.4806288	1.8021020
H	1.1602690	-0.4770898	2.7468930
H	-0.2839420	0.1076102	1.9233060
C	1.5310230	0.0935392	0.7078080
H	2.4623950	-0.4722628	0.7025270
H	1.7805020	1.1221112	0.9728780
C	0.9482560	0.0622702	-0.7028850
H	0.7399050	-0.9659388	-1.0051630
H	-0.4870130	1.5659532	-0.0179630
H	1.6932740	0.4371382	-1.4039630
O	-0.9607660	-2.2574218	1.0615970
O	-1.8839030	-1.2384688	1.0884110
O	1.0908310	-2.8163638	1.5569540
C	-0.2964750	0.9431582	-0.8993300
C	-1.5461970	0.0824082	-1.0841820
H	-1.7719870	-0.6170858	-0.0664240
O	-2.2552720	0.0457672	-2.0266420
O	-0.0584330	1.7543452	-2.0172440
O	-1.0961710	2.7192752	-2.0980370
H	-1.6889630	2.3145512	-2.7439550

$C_6H_9O_6$ 1,7 H-shift TS

C	2.0131868	-0.8014105	0.1744345
C	1.8865258	0.6985615	0.1334465
H	2.8698248	1.0459595	-0.1753055
H	1.6625248	1.1014465	1.1176435
C	0.8539018	1.1758355	-0.9062905
H	0.9588938	0.5770205	-1.8108295
H	1.1187538	2.1963495	-1.1810015
C	-0.6078412	1.2016525	-0.4564385
H	-1.2214972	1.5695875	-1.2823025
H	-0.5608162	-0.3998955	1.0632655
H	-0.7473792	1.9034615	0.3662315
O	1.2117588	-1.5151605	1.0594145
O	0.4157748	-0.7412415	1.8666085
O	2.7218818	-1.4591615	-0.5186535
C	-1.1716612	-0.1206165	0.0121805
C	-2.6076942	-0.0971775	0.4761365
H	-3.1915142	-1.0034035	0.2513845

O	-3.0704232	0.8415495	1.0620305
O	-0.8542712	-1.1136315	-0.8922255
O	-1.2554412	-2.3752795	-0.3746405
H	-0.4244882	-2.6844455	0.0149105

$C_6H_9O_6$ 1,8 H-shift product

C	2.5253058	0.0093651	0.0902010
C	1.6017688	1.0204331	-0.5292320
H	1.5793088	0.8685911	-1.6083130
H	2.0595508	1.9973591	-0.3592900
C	0.2036718	0.9852941	0.0758440
H	-0.3614522	1.8317881	-0.3107990
H	0.2777198	1.1116121	1.1568320
C	-0.5346422	-0.3124099	-0.2349490
H	0.0100728	-1.1663899	0.1694000
H	-1.8968802	-0.1655229	1.4438290
H	-0.6112472	-0.4570669	-1.3153720
O	3.4710718	-0.3788079	-0.7765960
O	2.4820378	-0.4161049	1.2171180
C	-1.9321222	-0.3416159	0.3638060
C	-2.5692962	-1.7290939	0.1902730
O	-3.6182852	-1.9697209	-0.2797370
O	-2.6863542	0.6647421	-0.2671430
O	-3.8929312	0.8478861	0.4544730
H	-4.4930542	0.2513031	-0.0114950
O	4.3799268	-1.2852129	-0.1846640
H	4.0058308	-1.3664279	0.7158150

$C_6H_9O_6$ 1,7 H-shift product

C	2.0191544	-0.1677872	0.2272037
C	1.0182214	0.8195978	0.7473687
C	0.1757724	1.4377188	-0.3771003
C	-0.7279436	0.4445138	-1.1217363
C	-1.7183686	-0.2312052	-0.2341993
C	-1.6677066	-1.6014842	0.0968797
O	-2.4919726	-2.1690082	0.8426877
O	-2.6344566	0.6116118	0.2182587
O	-3.5903726	0.1047258	1.1303047
H	-3.3667176	-0.8683382	1.1763817

O	1.7869464	-1.2482132	-0.2597033
O	3.2696614	0.2985798	0.3384557
O	4.2157464	-0.6132072	-0.1801043
H	3.6354614	-1.3501822	-0.4590353
H	0.3761814	0.2860718	1.4497957
H	1.5380394	1.6042988	1.2922407
H	0.8319124	1.9230048	-1.1004723
H	-1.2646026	0.9842058	-1.9040583
H	-0.1293486	-0.3258112	-1.6044183
H	-0.4411646	2.2196428	0.0644377
H	-0.8344436	-2.1587352	-0.3431873

$C_6H_9O_6$ CO loss TS

C	1.9043726	-0.3534020	0.3125963
C	1.1390106	0.8238700	0.8292883
C	0.2553026	1.4606000	-0.2574917
C	-0.8789574	0.5788890	-0.7961907
C	-1.8835334	0.1834530	0.2398823
O	1.5151036	-1.4992360	0.2283033
O	3.1234916	-0.0086850	-0.1008337
O	3.8350766	-1.1014810	-0.6430097
H	3.1927496	-1.8292610	-0.5266617
H	1.8446556	1.5642180	1.2012323
H	0.5291626	0.4710210	1.6595343
H	0.8869726	1.7774950	-1.0893217
H	-0.1715844	2.3686690	0.1711553
H	-1.4107644	1.1374380	-1.5668177
H	-0.4874574	-0.3143470	-1.2827417
O	-1.6143484	-0.8255920	1.1114723
O	-1.2339624	-2.0066450	0.4075313
H	-0.2616794	-1.9538540	0.4427233
H	-2.3541944	0.9800090	0.8102983
C	-3.5980034	-0.4038130	-0.8700027
O	-4.3314124	-1.0493460	-0.2809457

$C_6H_9O_8$ reactant

C	2.2594118	-0.0145370	0.0666580
C	1.4461558	1.2475740	0.1009180
H	2.1540308	2.0750150	0.0248150

785	H	0.9593508	1.3413330	1.0704130
786	C	0.4471818	1.3274980	-1.0516570
787	H	0.9922588	1.3546450	-1.9944930
788	H	-0.0952322	2.2668940	-0.9618140
789	C	-0.5384212	0.1611090	-1.1170730
790	H	-0.0077502	-0.7595370	-1.3566300
791	H	-0.6393722	-0.2855240	1.0128600
792	H	-1.2549472	0.3417480	-1.9192550
793	O	2.4464358	-0.5068940	1.2990920
794	O	2.7135338	-0.5538700	-0.9107980
795	C	-1.3114452	-0.0593060	0.1835730
796	O	-2.0154562	1.1280980	0.4381170
797	O	-2.6080892	1.0286570	1.7251460
798	H	-3.5142062	0.7844000	1.4983830
799	O	3.2414768	-1.6745610	1.2785800
800	H	3.3919778	-1.7833810	0.3178210
801	C	-2.3058812	-1.2009870	0.0400200
802	O	-3.4770402	-1.1100180	-0.0957450
803	O	-1.7873752	-2.5206350	0.0717060
804	O	-0.4965982	-2.5877200	0.2793640
805				
806	$C_6H_9O_8$ 1,4 H-shift TS			
807	C	2.2229443	0.0621679	0.1368969
808	C	1.1788303	0.8331299	0.8901669
809	H	1.7139323	1.5291999	1.5398479
810	H	0.6345003	0.1580649	1.5479599
811	C	0.2357393	1.6159089	-0.0174481
812	H	0.8032413	2.3639269	-0.5701081
813	H	-0.4644907	2.1531809	0.6220209
814	C	-0.5405217	0.7882089	-1.0509631
815	H	0.1402683	0.3967549	-1.8070861
816	H	-2.2752417	-0.6208561	-1.2524661
817	H	-1.2491527	1.4398419	-1.5613801
818	O	2.6793963	-0.9671381	0.8636739
819	O	2.6489053	0.3015359	-0.9653931
820	C	-1.3181117	-0.3869271	-0.4993741
821	O	-0.4789247	-1.4423081	-0.3009891
822	O	-1.2203477	-2.5316441	0.2306229
823	H	-0.8409527	-2.6051231	1.1153349

O	3.6999203	-1.6718151	0.1855989
H	3.7417233	-1.1777481	-0.6578631
C	-2.2576677	-0.0831431	0.6724549
O	-1.9659747	0.0271949	1.8207259
O	-3.5082567	0.0789939	0.2066979
O	-3.5797587	-0.2614061	-1.1489311

$C_6H_9O_8$ 1,5 H-shift TS

C	2.6181002	-0.0029391	-0.0911303
C	1.7954332	1.1613369	-0.5702213
H	1.7151682	1.1216099	-1.6564103
H	2.3615902	2.0638029	-0.3323753
C	0.4274272	1.2130119	0.0957777
H	-0.0645938	2.1495729	-0.1843103
H	0.5410352	1.2305089	1.1807557
C	-0.4819778	0.0855729	-0.3002423
H	-0.0965998	-1.0149641	0.2788097
H	-1.8082688	0.3652889	1.3623787
H	-0.4799628	-0.1663471	-1.3611393
O	3.5666512	-0.3234471	-0.9785613
O	2.4906382	-0.5899721	0.9529467
C	-1.8637828	0.0902669	0.3043507
O	-2.6476278	1.0184469	-0.4009733
O	-3.8538068	1.2281309	0.3205777
H	-4.3798578	0.4684889	0.0299207
O	4.3802592	-1.3813391	-0.5134983
H	3.9560972	-1.5869331	0.3437837
C	-2.4876618	-1.3048131	0.2029737
O	-3.6049458	-1.5293341	-0.1506433
O	-1.6562348	-2.3433871	0.4671037
O	-0.4270798	-1.9525621	1.0001257

$C_6H_9O_8$ 1,6 H-shift TS

C	2.7943931	0.0018830	-0.0136164
C	1.4653341	0.7000340	-0.1171904
H	1.6488631	1.6504470	-0.6314544
H	1.1078271	0.9557010	0.8805046
C	0.4538141	-0.1014540	-0.8928544

H	0.2279941	-1.1330140	-0.1304144
H	0.8548851	-0.5558350	-1.7942994
C	-0.9150359	0.5200870	-1.0342924
H	-1.4302169	0.1195800	-1.9058964
H	-1.2565399	0.5083180	1.1278156
H	-0.8239949	1.5993550	-1.1822484
O	3.4723761	0.4255940	1.0579736
O	3.2375291	-0.8129830	-0.7798064
C	-1.8098089	0.3280830	0.2039726
O	-2.8428389	1.2647700	0.0645986
O	-3.6451699	1.2214790	1.2341606
H	-4.2900429	0.5422700	0.9916706
O	4.7491641	-0.1734010	1.1385276
H	4.7316291	-0.7711120	0.3647496
C	-2.3955289	-1.0832030	0.2203536
O	-3.5456889	-1.3401040	0.0378976
O	-1.5241239	-2.1237290	0.3578496
O	-0.2648189	-1.7427650	0.8019986

$C_6H_9O_8$ 1,7 H-shift TS

C	-2.1953498	-0.1106593	0.2309493
C	-1.4212908	0.6173677	-0.7988567
H	-2.0398918	0.9435487	-1.6308067
H	-0.7541168	-0.3427623	-1.3804327
C	-0.3768318	1.6089707	-0.3537997
H	-0.8905138	2.4177787	0.1750533
H	0.0562102	2.0570667	-1.2492117
C	0.7450292	1.1080057	0.5583603
H	0.3389242	0.6981467	1.4800483
H	1.8838312	0.2947107	-1.1262047
H	1.3494502	1.9725887	0.8325333
O	-3.2961738	-0.6576623	-0.3073587
O	-1.9165308	-0.2462323	1.3974933
C	1.7364882	0.1110997	-0.0616347
O	2.9388382	0.3359097	0.6346923
O	3.9423482	-0.4978373	0.0759453
H	3.9157702	-1.2528923	0.6780153
O	-4.0283578	-1.3929723	0.6462493
H	-3.4737638	-1.2825303	1.4447453

C	1.3130452	-1.3406363	0.1656473
O	1.7099572	-2.0339453	1.0462393
O	0.3803032	-1.8956523	-0.6833277
O	0.0826252	-1.1114123	-1.7743397

$C_6H_9O_8$ 1,6 H-shift product

C	2.1774067	0.0521158	-0.0875762
O	2.0428057	1.2551418	-0.1078452
C	1.5051287	-0.9245942	0.8449968
C	0.2462917	-1.4598292	0.2417038
C	-1.0853983	-1.2968392	0.8832188
C	-1.9906533	-0.2632582	0.1869308
C	-1.2461583	1.0514998	-0.0506842
O	-1.0670673	1.5616218	-1.1154962
O	-2.3656693	-0.8278272	-1.0402522
O	-3.3424443	0.0081038	-1.6427152
H	-2.7799643	0.6672488	-2.0749742
O	2.9598757	-0.5756022	-0.9618662
O	3.5439637	0.3094698	-1.8946612
H	3.1700407	1.1671968	-1.6128432
O	-0.7884573	1.5124948	1.1295118
O	-0.0740083	2.7253978	1.0052018
H	0.7595957	2.4072728	0.6099578
H	-2.8753163	-0.0660822	0.7986538
H	-1.6356133	-2.2403642	0.8648708
H	-0.9785293	-0.9943592	1.9243578
H	0.3096277	-1.9416502	-0.7241242
H	2.2127337	-1.7337582	1.0507388
H	1.3018087	-0.3933992	1.7728948

$C_6H_9O_8$ 1,7 H-shift product

C	2.5881395	0.0546671	-0.1178608
O	3.0338975	0.0338101	1.0141972
C	1.3505195	0.6466001	-0.5422348
C	0.4594515	1.2875541	0.4550862
C	-0.2928635	0.2850191	1.3527482
C	-1.2114975	-0.6827999	0.6098272
C	-2.1301325	0.0544861	-0.3550298

O	-2.0417845	0.0661201	-1.5565128
O	-0.3942845	-1.5758419	-0.0987858
O	-1.2202545	-2.5809949	-0.6685518
H	-1.3477845	-2.2381099	-1.5623588
O	3.2560075	-0.5085039	-1.1488278
O	4.4675045	-1.0800789	-0.7125508
H	4.4323565	-0.8838909	0.2467342
O	-3.0689705	0.7347441	0.3042962
O	-3.9033875	1.4660791	-0.5719028
H	-3.5399705	1.2109651	-1.4429538
H	-1.8297135	-1.2298639	1.3256082
H	0.4226265	-0.3107039	1.9178722
H	-0.8991025	0.8415021	2.0665672
H	1.0574635	1.9144931	1.1192982
H	-0.2533315	1.9360441	-0.0552578
H	1.0651105	0.5587041	-1.5794078

Table S6 Conformers of the reactant for the $C_6H_9O_4$ 1,7 H-shift.

Conformer number	Vibrational partition function	Rotational partition function	Electronic energy incl. ZPVE in Hartees	Relative energy in kcal/mol
M001	1.67E+04	1.00E+06	-534.674067	1.77
M011	2.08E+04	9.94E+05	-534.674906	1.24
M015	1.58E+04	1.07E+06	-534.673752	1.97
M020	1.76E+04	1.03E+06	-534.674682	1.38
M035	1.69E+04	1.10E+06	-534.674908	1.24
M036	1.43E+04	1.10E+06	-534.674559	1.46
M037	1.04E+04	1.02E+06	-534.674988	1.19
M048	1.15E+04	1.02E+06	-534.674565	1.46
M050	9.89E+03	1.04E+06	-534.676653	0.15
M054	2.44E+04	1.06E+06	-534.674911	1.24
M070	2.15E+04	1.17E+06	-534.674918	1.23
M083	7.79E+03	9.84E+05	-534.675994	0.56
M092	1.85E+04	1.00E+06	-534.674807	1.30
M095	9.16E+03	9.09E+05	-534.67587	0.64
M111	1.37E+04	9.96E+05	-534.676885	0
M117	2.07E+04	1.09E+06	-534.674329	1.60
M119	1.53E+04	1.10E+06	-534.674383	1.57
M123	8.68E+03	9.58E+05	-534.674717	1.36
M124	9.58E+03	9.51E+05	-534.676824	0.04
M125	7.79E+03	9.62E+05	-534.675482	0.88
M129	8.37E+03	9.57E+05	-534.674357	1.59
M143	1.12E+04	9.91E+05	-534.674639	1.41
M150	1.37E+04	1.04E+06	-534.675077	1.13
M157	1.79E+04	9.51E+05	-534.674872	1.26
M162	2.22E+04	1.09E+06	-534.673387	2.20
M183	2.66E+04	1.06E+06	-534.67401	1.80
M188	6.63E+03	9.04E+05	-534.674828	1.29
M194	1.04E+04	1.04E+06	-534.674861	1.27
M212	5.31E+03	8.49E+05	-534.675472	0.89
M216	1.66E+04	9.78E+05	-534.675398	0.93
M226	1.30E+04	9.06E+05	-534.675402	0.93
M235	1.06E+04	1.03E+06	-534.67606	0.52
M248	7.55E+03	9.19E+05	-534.67578	0.69
M263	9.24E+03	8.46E+05	-534.67582	0.67
M286	1.20E+04	9.91E+05	-534.675488	0.88
M290	1.07E+04	9.27E+05	-534.675767	0.70
M292	3.33E+04	8.89E+05	-534.675377	0.95
M298	2.07E+04	1.02E+06	-534.675785	0.69
M322	8.30E+03	9.41E+05	-534.676192	0.43
M330	9.63E+03	7.82E+05	-534.675413	0.92
M337	2.18E+04	1.06E+06	-534.675064	1.14

M372	1.98E+04	1.17E+06	-534.674754	1.34
M373	1.39E+04	9.93E+05	-534.675706	0.74
M380	8.59E+03	9.02E+05	-534.675244	1.03
M387	1.07E+04	7.86E+05	-534.675367	0.95
M392	1.21E+04	8.25E+05	-534.675354	0.96
M402	3.16E+03	7.42E+05	-534.676346	0.34
M403	1.30E+04	1.11E+06	-534.676659	0.14
M440	6.73E+03	9.41E+05	-534.67444	1.53
M453	2.64E+03	7.30E+05	-534.676777	0.07
M456	9.27E+03	8.43E+05	-534.674672	1.39
M462	1.05E+04	9.89E+05	-534.676516	0.23
M496	1.55E+04	9.32E+05	-534.674611	1.43
M505	3.30E+04	1.07E+06	-534.674139	1.72
M506	5.03E+03	8.58E+05	-534.675254	1.02
M527	2.10E+03	6.90E+05	-534.6762	0.43
M542	2.20E+03	6.46E+05	-534.67638	0.32
M545	2.25E+04	9.23E+05	-534.675854	0.65
M548	2.43E+03	7.18E+05	-534.676316	0.36

991 **Table S7** Conformers of the transition state for the $C_6H_9O_4$ 1,7 H-shift.

Conformer number	Vibrational partition function	Rotational partition function	Electronic energy incl. ZPVE in Hartees	Relative energy in kcal/mol
107	1.21E+03	7.52E+05	-534.651653	1.78
152	1.35E+03	7.57E+05	-534.652989	0.95
172	1.15E+03	7.10E+05	-534.652814	1.06
177	1.89E+03	7.79E+05	-534.652732	1.11
19	5.77E+02	7.05E+05	-534.652944	0.97
1	7.27E+02	6.75E+05	-534.650137	2.74
249	2.09E+03	7.68E+05	-534.647726	4.25
25	6.24E+02	7.27E+05	-534.654497	0
274	6.65E+02	6.68E+05	-534.647883	4.15
285	5.39E+02	6.67E+05	-534.647666	4.29
4	5.35E+02	7.10E+05	-534.648387	3.83
91	9.95E+02	7.38E+05	-534.647938	4.12

992
993

Table S8 Conformers of the product for the $C_6H_9O_4$ 1,7 H-shift and also the reactant of $C_6H_9O_4$ CO loss.

Conformer number	Vibrational partition function	Rotational partition function	Electronic energy incl. ZPVE in Hartees	Relative energy in kcal/mol
M001	1.44E+04	9.97E+05	-534.667011	1.72
M003	1.68E+04	1.00E+06	-534.667312	1.53
M009	1.45E+04	9.29E+05	-534.667125	1.65
M014	3.22E+04	1.10E+06	-534.667077	1.68
M019	3.25E+04	1.10E+06	-534.667180	1.61
M020	2.03E+04	1.01E+06	-534.667204	1.60
M025	2.27E+04	1.04E+06	-534.667019	1.71
M035	4.59E+04	1.19E+06	-534.666702	1.91
M043	2.40E+04	1.11E+06	-534.666723	1.90
M069	2.62E+04	1.10E+06	-534.666741	1.89
M086	2.63E+04	1.10E+06	-534.666742	1.89
M129	2.43E+04	1.00E+06	-534.666986	1.73
M133	2.25E+04	1.04E+06	-534.666776	1.86
M146	3.71E+04	1.18E+06	-534.666672	1.93
M147	2.11E+04	1.08E+06	-534.666821	1.84
M148	1.28E+04	9.35E+05	-534.669259	0.31
M167	1.25E+04	9.48E+05	-534.668303	0.91
M173	9.13E+03	9.54E+05	-534.667595	1.35
M181	8.65E+03	1.02E+06	-534.668384	0.86
M192	9.63E+03	9.80E+05	-534.668818	0.58
M209	5.43E+03	7.60E+05	-534.668914	0.52
M212	2.79E+04	1.02E+06	-534.666695	1.92
M227	3.19E+04	9.99E+05	-534.666609	1.97
M246	1.69E+04	1.03E+06	-534.666429	2.08
M265	5.81E+03	7.86E+05	-534.668635	0.70
M273	1.14E+04	1.02E+06	-534.666622	1.96
M314	1.52E+04	1.03E+06	-534.666585	1.98
M338	5.34E+03	7.66E+05	-534.669026	0.45
M346	2.25E+04	1.04E+06	-534.666775	1.87
M386	2.34E+03	7.26E+05	-534.669748	0
M390	2.73E+04	1.05E+06	-534.666837	1.83
M539	1.22E+04	8.25E+05	-534.668904	0.53
M547	1.14E+04	1.01E+06	-534.669464	0.18
M675	1.39E+04	9.10E+05	-534.668110	1.03

Table S9 Conformers of the transition state of $C_6H_9O_4$ CO loss.

Conformer number	Vibrational partition function	Rotational partition function	Electronic energy incl. ZPVE in Hartees	Relative energy in kcal/mol
M01	2.35E+04	8.17E+05	-534.643885	0.44
M03	1.67E+04	8.27E+05	-534.643456	0.71
M09	1.04E+04	8.40E+05	-534.642906	1.05
M10	4.81E+04	8.74E+05	-534.642020	1.61
M12	2.42E+04	8.01E+05	-534.642863	1.08
M13-	1.35E+04	9.23E+05	-534.644017	0.36
M14	1.80E+04	9.04E+05	-534.644586	0
M17	1.35E+04	9.23E+05	-534.644018	0.36
M21	2.34E+04	9.55E+05	-534.643479	0.69
M25	3.24E+04	1.01E+06	-534.644118	0.29
M27	6.16E+04	1.02E+06	-534.642474	1.33
M28	2.17E+04	9.82E+05	-534.644304	0.18
M43	1.09E+04	8.58E+05	-534.643170	0.89
M44	1.35E+04	8.80E+05	-534.642984	1.01
M53-	7.25E+04	9.79E+05	-534.642253	1.46
M63	2.04E+05	1.21E+06	-534.641669	1.83
M67	4.55E+04	1.10E+06	-534.643355	0.77
M70	8.26E+04	1.03E+06	-534.641673	1.83
M74-	6.38E+04	1.16E+06	-534.641783	1.76
M75	1.18E+05	1.14E+06	-534.640900	2.31

Table S10 Conformers of the reactant for the $C_6H_9O_6$ 1,8 H-shift and 1,7 H-shift.

Conformer number	Vibrational partition function	Rotational partition function	Electronic energy incl. ZPVE in Hartees	Relative energy in kcal/mol
M012	4.84E+04	1.47E+06	-685.049415	1.77
M032	2.61E+04	1.26E+06	-685.051564	0.42
M039	1.36E+04	1.36E+06	-685.050459	1.12
M043	1.19E+04	1.36E+06	-685.051868	0.23
M066	1.70E+04	1.53E+06	-685.050893	0.84
M071	1.84E+04	1.52E+06	-685.052093	0.09
M087	2.83E+04	1.53E+06	-685.051497	0.47
M121	7.95E+04	1.78E+06	-685.05018	1.29
M222	1.50E+05	1.97E+06	-685.048624	2.27
M227	6.77E+04	1.93E+06	-685.049899	1.47
M273	2.51E+04	1.50E+06	-685.050332	1.20
M329	7.31E+04	1.61E+06	-685.0509	0.84
M372	2.67E+05	2.08E+06	-685.0485	2.35
M385	5.68E+04	1.77E+06	-685.050996	0.78
M387	7.26E+04	1.94E+06	-685.047824	2.77
M528	1.73E+05	1.85E+06	-685.048334	2.45
M546	2.33E+05	1.87E+06	-685.048301	2.47
M572	2.12E+04	1.23E+06	-685.052239	0
M666	5.87E+04	1.57E+06	-685.050473	1.11
M703	1.04E+05	1.84E+06	-685.048644	2.26
M961	1.88E+05	2.07E+06	-685.049039	2.01

Table S11 Conformers of the transition state for the $C_6H_9O_6$ 1,8 H-shift.

Conformer number	Vibrational partition function	Rotational partition function	Electronic energy incl. ZPVE in Hartees	Relative energy in kcal/mol
M114	3.12E+03	1.23E+06	-685.028291	1.35
M189	3.16E+03	1.30E+06	-685.030442	0
M220	2.46E+03	1.20E+06	-685.028390	1.29
M266	1.43E+03	9.86E+05	-685.027391	1.91
M341	1.76E+03	1.01E+06	-685.028846	1.00
M369	3.88E+03	1.26E+06	-685.029924	0.33
M400	3.02E+03	1.29E+06	-685.028979	0.92
M482	3.04E+03	1.24E+06	-685.028666	1.11
M693	1.88E+03	1.18E+06	-685.027469	1.87

Table S12 Conformers of the transition state for the $C_6H_9O_6$ 1,7 H-shift.

Conformer number	Vibrational partition function	Rotational partition function	Electronic energy incl. ZPVE in Hartees	Relative energy in kcal/mol
M031	2.50E+03	1.09E+06	-685.030071	0
M034	2.50E+03	1.09E+06	-685.030070	0.00
M061	2.75E+03	1.18E+06	-685.029012	0.66
M064	4.11E+03	1.16E+06	-685.026928	1.97
M076	4.97E+03	1.20E+06	-685.025618	2.79
M080	4.11E+03	1.16E+06	-685.026929	1.97
M151	3.36E+03	1.13E+06	-685.027051	1.90

Table S13 Conformers of the product for the $C_6H_9O_6$ 1,8 H-shift and reactant for the $C_6H_9O_6$ CO loss.

Conformer number	Vibrational partition function	Rotational partition function	Electronic energy incl. ZPVE in Hartees	Relative energy in kcal/mol
M004	1.97E+05	1.72E+06	-685.056826	1.04
M013	2.38E+05	1.77E+06	-685.057240	0.78
M017	1.18E+05	1.54E+06	-685.058315	0.11
M018	1.18E+05	1.54E+06	-685.058316	0.11
M020	1.18E+05	1.82E+06	-685.058486	0
M024	7.86E+05	2.09E+06	-685.052147	3.98
M027	1.42E+05	1.83E+06	-685.057552	0.59
M028	1.10E+05	1.49E+06	-685.057268	0.76
M041	3.12E+05	1.78E+06	-685.055345	1.97
M049	4.86E+05	1.96E+06	-685.055532	1.85
M051	2.43E+05	1.91E+06	-685.057042	0.91
M052	3.21E+05	1.82E+06	-685.056130	1.48
M059	1.20E+05	1.69E+06	-685.055747	1.72
M064	1.64E+05	1.69E+06	-685.056849	1.03
M075	1.49E+05	1.72E+06	-685.056637	1.16
M079	1.41E+05	1.69E+06	-685.056786	1.07
M100	1.74E+05	1.94E+06	-685.048537	6.24
M130	1.95E+05	1.97E+06	-685.047048	7.18
M132	2.20E+05	2.09E+06	-685.048944	5.99
M144	1.80E+05	1.99E+06	-685.048677	6.16
M161	1.47E+05	1.74E+06	-685.048367	6.35
M182	2.19E+04	1.54E+06	-685.050543	4.98
M187	1.90E+05	2.00E+06	-685.046868	7.29
M191	2.78E+04	1.35E+06	-685.056543	1.22
M205	1.38E+05	1.82E+06	-685.049251	5.80
M221	1.64E+05	1.81E+06	-685.048094	6.52
M223	1.40E+05	1.79E+06	-685.048408	6.32
M246	1.61E+05	1.86E+06	-685.048799	6.08
M263	1.83E+05	1.87E+06	-685.049539	5.61
M303	1.49E+05	1.85E+06	-685.048705	6.14
M388	1.88E+05	1.64E+06	-685.049116	5.88
M407	2.44E+05	1.81E+06	-685.048620	6.19
M413	2.85E+04	1.30E+06	-685.057673	0.51
M428	1.50E+05	1.62E+06	-685.048623	6.19
M454	1.41E+05	1.65E+06	-685.048327	6.37
M487	1.36E+05	1.75E+06	-685.048356	6.36
M503	1.29E+05	1.85E+06	-685.048663	6.16
M505	1.72E+04	1.26E+06	-685.049405	5.70
M507	1.92E+04	1.27E+06	-685.049954	5.35
M547	1.66E+04	1.36E+06	-685.049022	5.94
M550	9.70E+03	1.21E+06	-685.049190	5.83

M584	3.52E+04	1.23E+06	-685.049417	5.69
M618	1.66E+04	1.36E+06	-685.049023	5.94
M657	1.57E+04	1.21E+06	-685.049757	5.48
M004	5.73E+04	1.39E+06	-685.056436	1.29
M011	7.22E+04	1.36E+06	-685.056814	1.05
M021	1.50E+05	1.52E+06	-685.055627	1.79
M034	2.39E+04	1.77E+06	-685.054497	2.50
M035	2.67E+04	1.40E+06	-685.056324	1.36
M042	1.74E+05	1.87E+06	-685.056164	1.46
M055	1.95E+05	1.79E+06	-685.055014	2.18
M059	2.84E+05	1.81E+06	-685.056181	1.45
M064	2.71E+05	1.78E+06	-685.055851	1.65
M083	2.00E+05	1.68E+06	-685.055878	1.64
M096	2.40E+05	1.87E+06	-685.056383	1.32
M100	2.90E+05	1.87E+06	-685.056614	1.17
M109	1.70E+05	1.82E+06	-685.058029	0.29
M146	7.12E+04	1.52E+06	-685.057848	0.40
M161	3.62E+05	2.07E+06	-685.057066	0.89
M163	2.59E+05	2.07E+06	-685.057312	0.74
M174	2.45E+04	1.95E+06	-685.057178	0.82
M272	4.10E+05	1.73E+06	-685.056722	1.11
M303	2.21E+05	1.86E+06	-685.058152	0.21
M350	2.06E+05	1.82E+06	-685.056596	1.19
M420	1.93E+05	1.88E+06	-685.057483	0.63
M516	3.00E+05	1.90E+06	-685.056702	1.12
M598	8.96E+04	1.49E+06	-685.057899	0.37
M622	1.75E+05	1.55E+06	-685.057870	0.39
M748	2.25E+05	1.93E+06	-685.055852	1.65
M808	2.04E+05	1.78E+06	-685.056119	1.49
M856	2.03E+05	1.75E+06	-685.055899	1.62
M914	1.73E+05	1.83E+06	-685.056491	1.25

1011
1012

1013 **Table S14** Conformers of the product for the $C_6H_9O_6$ 1,7 H-shift.

Conformer number	Vibrational partition function	Rotational partition function	Electronic energy incl. ZPVE in Hartees	Relative energy in kcal/mol
M006	2.82E+04	1.22E+06	-685.071137	3.32
M042	2.38E+03	9.79E+05	-685.073271	1.98
M044	6.60E+04	1.49E+06	-685.076425	0.00
M132	1.51E+05	1.81E+06	-685.074789	1.03
M059	1.61E+04	1.03E+06	-685.072684	2.35
M104	1.89E+04	1.12E+06	-685.070558	3.68

1014
1015
1016

Table S15 Conformers of the transition state for the $C_6H_9O_6$ CO loss.

Conformer number	Vibrational partition function	Rotational partition function	Electronic energy incl. ZPVE in Hartees	Relative energy in kcal/mol
M002	9.69E+04	1.40E+06	-685.043171	0.52
M003	1.80E+06	2.01E+06	-685.040855	1.97
M004	8.64E+05	2.24E+06	-685.043070	0.58
M005	6.26E+05	2.09E+06	-685.042810	0.74
M006	6.72E+04	1.32E+06	-685.041896	1.32
M008	6.91E+05	2.07E+06	-685.042621	0.86
M010	6.81E+05	1.98E+06	-685.042989	0.63
M013	7.20E+05	2.24E+06	-685.042784	0.76
M014	4.39E+05	1.70E+06	-685.041682	1.45
M005	5.31E+05	1.92E+06	-685.042297	1.07
M007	8.07E+05	1.92E+06	-685.041468	1.59
M009	5.92E+05	1.69E+06	-685.041388	1.64
M011	4.82E+05	1.64E+06	-685.042254	1.09
M012	8.98E+05	1.79E+06	-685.040994	1.88
M033	5.36E+04	1.46E+06	-685.043997	0
M034	7.38E+04	1.50E+06	-685.043714	0.18
M034	1.14E+05	1.62E+06	-685.042345	1.04
M040	4.29E+05	1.71E+06	-685.042109	1.18
M041	8.13E+05	1.93E+06	-685.041837	1.36
M049	3.89E+05	1.96E+06	-685.043252	0.47
M050	5.60E+05	1.87E+06	-685.041634	1.48
M075	7.49E+05	1.90E+06	-685.042089	1.20
M089	4.05E+05	1.90E+06	-685.043021	0.61
M095	6.70E+05	2.05E+06	-685.042853	0.72
M117	6.73E+05	1.75E+06	-685.042985	0.64
M142	5.97E+05	1.90E+06	-685.042611	0.87
M160	1.08E+06	1.84E+06	-685.041696	1.44
M161	5.98E+05	1.90E+06	-685.042612	0.87
M190	4.05E+05	1.90E+06	-685.043020	0.61
M211	1.08E+06	1.84E+06	-685.041698	1.44
M231	8.06E+05	2.01E+06	-685.042063	1.21
M246	4.02E+05	1.71E+06	-685.043537	0.29
M258	6.95E+05	2.01E+06	-685.042522	0.93
M259	5.00E+05	2.03E+06	-685.042321	1.05
M265	1.14E+06	1.79E+06	-685.042959	0.65
M298	6.26E+05	1.67E+06	-685.042323	1.05
M303	7.20E+05	2.24E+06	-685.042784	0.76
M328	5.98E+05	1.68E+06	-685.041474	1.58
M339	7.39E+05	1.77E+06	-685.042011	1.25
M340	1.79E+06	2.04E+06	-685.041850	1.35
M375	9.36E+05	2.08E+06	-685.042573	0.89

M386	3.84E+05	1.99E+06	-685.042931	0.67
M429	4.06E+05	1.74E+06	-685.043041	0.60
M433	5.91E+05	1.70E+06	-685.042846	0.72
M434	4.82E+05	2.01E+06	-685.043485	0.32
M460	6.60E+05	2.02E+06	-685.043085	0.57
M462	4.11E+05	1.67E+06	-685.042585	0.89
M487	1.24E+05	1.44E+06	-685.042210	1.12
M509	8.81E+05	1.94E+06	-685.042302	1.06
M538	6.69E+05	1.84E+06	-685.042632	0.86
M580	4.34E+05	2.01E+06	-685.043748	0.16
M581	6.29E+05	1.71E+06	-685.043602	0.25
M588	6.97E+05	1.72E+06	-685.043358	0.40
M613	8.63E+04	1.43E+06	-685.043395	0.38
M734	6.10E+05	1.97E+06	-685.042873	0.71
M790	4.10E+05	1.65E+06	-685.043187	0.51

Table S16 Conformers of the reactant for the $C_6H_9O_8$ 1,7 H-shift, 1.4 H-shift, 1,5 H-shift and 1,6 H-shift.

Conformer number	Vibrational partition function	Rotational partition function	Electronic energy incl. ZPVE in Hartees	Relative energy in kcal/mol
M017	5.09E+05	2.15E+06	-835.435129	0.40
M040	2.07E+06	2.76E+06	-835.434371	0.87
M062	1.37E+06	2.55E+06	-835.435462	0.19
M0020	3.24E+06	2.91E+06	-835.433048	1.70
M0026	4.62E+06	2.92E+06	-835.431993	2.36
M0042	4.71E+06	2.96E+06	-835.432021	2.35
M0056	4.85E+06	3.17E+06	-835.431996	2.36
M0110	6.48E+06	3.17E+06	-835.432568	2.00
M0186	3.18E+06	2.75E+06	-835.432783	1.87
M0201	5.64E+06	3.17E+06	-835.432767	1.88
M0253	4.98E+06	2.89E+06	-835.432402	2.11
M0274	3.57E+06	2.99E+06	-835.432932	1.77
M0294	4.21E+06	3.02E+06	-835.432707	1.92
M0299	2.95E+06	3.02E+06	-835.433419	1.47
M0370	3.15E+05	2.43E+06	-835.435034	0.45
M0459	3.30E+06	2.89E+06	-835.433156	1.63
M0466	4.82E+06	3.03E+06	-835.432599	1.98
M0712	2.78E+06	2.69E+06	-835.43299	1.74
M0776	2.69E+06	2.74E+06	-835.432757	1.88
M0844	4.76E+06	2.83E+06	-835.432284	2.18
M0859	3.46E+06	3.18E+06	-835.432865	1.82
M0896	2.13E+06	2.83E+06	-835.434183	0.99
M1022	3.20E+06	2.41E+06	-835.432888	1.80
M1084	6.70E+06	2.81E+06	-835.431881	2.43
M1094	2.07E+05	2.32E+06	-835.434454	0.82
M1114	2.34E+06	3.08E+06	-835.435669	0.06
M1123	6.21E+06	2.49E+06	-835.433243	1.58
M1245	3.64E+06	3.22E+06	-835.4348	0.60
M1254	1.83E+06	3.21E+06	-835.434834	0.58
M1262	2.78E+06	2.98E+06	-835.433791	1.23
M1338	1.42E+06	3.00E+06	-835.434412	0.85
M1339	3.10E+06	3.01E+06	-835.434475	0.81
M1362	1.91E+05	2.02E+06	-835.434003	1.10
M1789	2.43E+06	2.75E+06	-835.43476	0.63
M1791	1.79E+06	2.80E+06	-835.435658	0.06
M1930	3.09E+06	2.89E+06	-835.435268	0.31
M2327	1.05E+06	2.18E+06	-835.435759	0
M2419	7.52E+05	2.60E+06	-835.43439	0.86
M2525	2.02E+06	2.89E+06	-835.434505	0.79
M2533	4.33E+05	2.14E+06	-835.43561	0.09
M2960	9.16E+05	2.30E+06	-835.43528	0.30

M3029	2.37E+06	2.84E+06	-835.434129	1.02
M3030	1.76E+06	2.86E+06	-835.434169	1.00
M3293	7.83E+04	1.94E+06	-835.434566	0.75

Table S17 Conformers of the transition state for the $C_6H_9O_8$ 1,7 H-shift.

Conformer number	Vibrational partition function	Rotational partition function	Electronic energy incl. ZPVE in Hartees	Relative energy in kcal/mol
M001	5.20E+04	1.87E+06	-835.399864	3.74
M002	4.16E+04	1.85E+06	-835.398755	4.43
M002	6.75E+04	1.91E+06	-835.403292	1.59
M014	7.76E+04	1.96E+06	-835.405819	0.00
M018	6.12E+04	1.89E+06	-835.402376	2.16
M022	5.06E+04	1.95E+06	-835.404683	0.71

Table S18 Conformers of the transition state for the $C_6H_9O_8$ 1,6 H-shift.

Conformer number	Vibrational partition function	Rotational partition function	Electronic energy incl. ZPVE in Hartees	Relative energy in kcal/mol
M001	4.34E+04	2.09E+06	-835.395859	5.70
M002	1.73E+05	2.47E+06	-835.397249	4.83
M004	4.13E+04	1.87E+06	-835.396598	5.24
M005	4.85E+04	1.87E+06	-835.396372	5.38
M015	1.34E+05	2.54E+06	-835.404258	0.43
M017	1.90E+05	2.52E+06	-835.404943	0.00
M024	1.75E+05	2.42E+06	-835.402895	1.29
M068	1.35E+05	2.32E+06	-835.403966	0.61
M071	2.36E+05	2.59E+06	-835.404766	0.11
M118	1.12E+05	2.51E+06	-835.403913	0.65

Table S19 Conformers of the transition state for the $C_6H_9O_8$ 1,5 H-shift.

Conformer number	Vibrational partition function	Rotational partition function	Electronic energy incl. ZPVE in Hartees	Relative energy in kcal/mol
M005	2.54E+05	2.10E+06	-835.402026	0.21
M029	1.51E+05	2.14E+06	-835.399485	1.81
M047	1.54E+05	2.02E+06	-835.400130	1.40
M056	1.17E+05	2.10E+06	-835.400313	1.29
M032	2.58E+05	2.50E+06	-835.402364	0
M018	1.22E+06	2.15E+06	-835.395691	4.19
M021	1.52E+06	2.82E+06	-835.396649	3.59
M065	9.72E+05	2.23E+06	-835.394663	4.83
M075	1.14E+06	2.98E+06	-835.395693	4.19
M078	1.19E+06	2.61E+06	-835.397479	3.07
M123	1.85E+06	2.88E+06	-835.395038	4.60
M136	8.28E+05	2.63E+06	-835.396288	3.81
M151	1.31E+06	2.54E+06	-835.396115	3.92
M167	1.18E+06	2.54E+06	-835.395784	4.13
M168	1.06E+06	2.55E+06	-835.395663	4.20
M192	1.01E+06	2.51E+06	-835.396118	3.92
M252	1.41E+06	2.96E+06	-835.393976	5.26
M301	1.30E+06	2.38E+06	-835.395021	4.61

Table S20 Conformers of the transition state for the $C_6H_9O_8$ 1,4 H-shift.

Conformer number	Vibrational partition function	Rotational partition function	Electronic energy incl. ZPVE in Hartees	Relative energy in kcal/mol
M115	5.45E+05	2.16E+06	-835.403992	0.25
M120	7.18E+04	1.75E+06	-835.399104	3.32
M121	1.05E+05	1.80E+06	-835.399993	2.76
M124	1.18E+05	2.01E+06	-835.397158	4.54
M243	6.04E+04	1.65E+06	-835.399997	2.76
M303	7.32E+04	1.64E+06	-835.398274	3.84
M357	1.01E+05	1.97E+06	-835.399749	2.92
M019	1.57E+06	2.62E+06	-835.403500	0.56
M041	1.04E+06	2.80E+06	-835.403439	0.60
M058	1.26E+06	2.74E+06	-835.403201	0.75
M079	1.61E+06	2.69E+06	-835.402632	1.11
M097	1.04E+06	2.80E+06	-835.403440	0.60
M1093	9.11E+05	2.41E+06	-835.403555	0.53
M1133	9.85E+05	2.41E+06	-835.402013	1.49
M115	8.63E+05	2.60E+06	-835.403361	0.65
M120	1.01E+06	2.72E+06	-835.403662	0.46
M1321	8.65E+05	2.05E+06	-835.402554	1.16
M135	1.41E+06	3.05E+06	-835.402690	1.07
M1460	1.25E+06	2.58E+06	-835.401592	1.76

M151	2.77E+06	2.81E+06	-835.402635	1.10
M160	2.94E+06	2.82E+06	-835.400954	2.16
M192	1.43E+06	2.79E+06	-835.402486	1.20
M1941	1.14E+06	2.58E+06	-835.401703	1.69
M202	1.65E+06	2.64E+06	-835.401502	1.82
M216	2.72E+06	3.07E+06	-835.400985	2.14
M222	1.22E+06	2.94E+06	-835.402717	1.05
M250	1.04E+06	2.70E+06	-835.403205	0.75
M267	3.08E+06	2.83E+06	-835.401043	2.10
M296	1.58E+06	2.62E+06	-835.401378	1.89
M301	1.21E+06	2.68E+06	-835.403987	0.26
M322	2.90E+06	3.08E+06	-835.400978	2.14
M354	4.21E+06	2.93E+06	-835.402677	1.08
M453	1.04E+06	2.80E+06	-835.403441	0.60
M456	1.78E+06	2.77E+06	-835.401107	2.06
M514	8.36E+05	2.50E+06	-835.402797	1.00
M548	1.63E+05	2.02E+06	-835.402815	0.99
M625	1.39E+06	2.73E+06	-835.401975	1.52
M701	1.70E+06	2.76E+06	-835.401822	1.61
M727	2.95E+05	2.01E+06	-835.404395	0
M758	9.63E+05	2.28E+06	-835.403017	0.86
M780	1.20E+06	2.49E+06	-835.401164	2.03
M838	7.57E+05	2.07E+06	-835.402357	1.28
M856	4.15E+06	2.54E+06	-835.402584	1.14
M931	8.32E+05	2.47E+06	-835.401136	2.05
M949	6.39E+05	2.09E+06	-835.402406	1.25

Table 21 Conformers of the product for the $C_6H_9O_8$ 1,7 H-shift.

Conformer number	Vibrational partition function	Rotational partition function	Electronic energy incl. ZPVE in Hartees	Relative energy in kcal/mol
M000	1.49E+06	2.98E+06	-835.436576	1.40
M003	1.44E+06	3.13E+06	-835.437096	1.07
M007	5.78E+05	2.32E+06	-835.437399	0.88
M010	1.02E+06	3.04E+06	-835.436427	1.49
M012	1.69E+06	2.80E+06	-835.436149	1.67
M015	5.75E+06	3.17E+06	-835.435921	1.81
M016	7.36E+05	2.33E+06	-835.438204	0.38
M017	7.36E+05	2.33E+06	-835.438205	0.38
M019	1.06E+06	2.57E+06	-835.436976	1.15
M023	2.00E+06	3.01E+06	-835.436019	1.75
M029	3.93E+06	2.79E+06	-835.437333	0.93
M039	2.22E+06	3.23E+06	-835.438315	0.31
M047	1.45E+06	3.11E+06	-835.436338	1.55
M063	1.58E+06	2.80E+06	-835.436810	1.25

M069	7.79E+05	2.67E+06	-835.436754	1.29
M070	1.25E+06	2.59E+06	-835.437970	0.53
M071	2.48E+06	3.09E+06	-835.436656	1.35
M072	6.51E+05	2.28E+06	-835.438561	0.15
M079	2.73E+06	2.95E+06	-835.437986	0.52
M080	8.16E+05	2.26E+06	-835.436383	1.52
M091	2.18E+06	2.92E+06	-835.436527	1.43
M099	3.94E+06	2.79E+06	-835.437334	0.92
M102	2.81E+06	3.01E+06	-835.438007	0.50
M110	2.28E+06	3.06E+06	-835.436694	1.33
M111	1.35E+06	2.75E+06	-835.437382	0.89
M113	9.47E+05	2.29E+06	-835.437730	0.68
M115	9.46E+05	2.29E+06	-835.437729	0.68
M130	4.64E+06	3.38E+06	-835.437577	0.77
M143	1.14E+06	2.31E+06	-835.438808	0
M144	4.75E+05	2.06E+06	-835.438522	0.18
M147	5.63E+05	2.16E+06	-835.438226	0.37
M153	2.20E+05	2.52E+06	-835.436013	1.75
M158	3.49E+05	2.45E+06	-835.437600	0.76
M159	1.35E+06	3.05E+06	-835.435747	1.92
M162	2.37E+05	2.38E+06	-835.437695	0.70
M163	2.00E+06	3.37E+06	-835.436440	1.49
M087	9.29E+05	2.35E+06	-835.435830	1.87
M097	1.80E+06	2.77E+06	-835.435778	1.90
M108	6.72E+05	2.35E+06	-835.437630	0.74
M113	1.34E+06	2.96E+06	-835.434991	2.40
M114	1.02E+06	2.91E+06	-835.434771	2.53
M119	2.98E+05	2.40E+06	-835.437179	1.02
M121	2.57E+06	2.72E+06	-835.435209	2.26
M123	2.57E+06	2.72E+06	-835.435208	2.26
M139	2.81E+06	3.01E+06	-835.438008	0.50
M147	3.45E+06	3.23E+06	-835.436745	1.29
M148	1.63E+05	2.44E+06	-835.437511	0.81
M151	1.45E+06	3.13E+06	-835.437097	1.07
M152	8.35E+05	2.34E+06	-835.436421	1.50
M155	4.02E+06	3.31E+06	-835.434282	2.84
M176	1.84E+05	2.19E+06	-835.436641	1.36

Table 22 Conformers of the product for the $C_6H_9O_8$ 1,6 H-shift.

Conformer number	Vibrational partition function	Rotational partition function	Electronic energy incl. ZPVE in Hartees	Relative energy in kcal/mol
M113	1.11E+05	1.79E+06	-835.43014	0.24
M446	5.69E+05	2.30E+06	-835.42949	0.65
M454	1.26E+06	2.30E+06	-835.42983	0.43
M476	2.81E+06	2.38E+06	-835.42758	1.84
M478	8.00E+05	2.24E+06	-835.42965	0.55
M490	9.53E+05	2.20E+06	-835.42922	0.82
M026	2.64E+06	2.32E+06	-835.42709	2.15
M057	4.02E+06	2.73E+06	-835.42862	1.19
M1001	3.49E+06	2.98E+06	-835.42934	0.74
M1064	1.35E+05	1.78E+06	-835.42896	0.98
M1146	1.33E+06	2.61E+06	-835.42941	0.70
M1170	4.02E+06	2.73E+06	-835.42862	1.19
M1285	2.82E+06	2.80E+06	-835.42970	0.51
M1300	2.14E+05	2.05E+06	-835.43052	0
M1414	8.11E+06	2.99E+06	-835.42920	0.82
M1417	3.42E+06	2.93E+06	-835.42923	0.81
M150	1.08E+06	2.22E+06	-835.42750	1.89
M171	5.40E+06	2.92E+06	-835.42793	1.63
M1735	5.93E+06	3.16E+06	-835.42754	1.87
M173	2.82E+06	2.72E+06	-835.42957	0.59
M267	6.60E+05	2.40E+06	-835.42955	0.61
M321	5.56E+06	2.68E+06	-835.42805	1.55
M333	1.12E+06	2.25E+06	-835.42742	1.94
M398	4.11E+06	3.25E+06	-835.42788	1.66
M477	6.75E+06	3.40E+06	-835.42840	1.33
M492	2.83E+06	2.72E+06	-835.42957	0.59
M539	2.91E+06	2.88E+06	-835.42844	1.31
M790	4.13E+05	1.81E+06	-835.42751	1.89
M863	5.14E+06	2.53E+06	-835.42802	1.57
M903	3.08E+06	2.61E+06	-835.42823	1.44
M965	3.07E+06	2.85E+06	-835.42801	1.57

References that appear only in the SI:

[91] Kürten, A.; Rondo, L.; Ehrhart, S.; Curtius J. *J. Phys. Chem. A* **2012**, *116*, 6375-6386.

[92] Docherty, K. S.; Ziemann, P. J. *Aerosol Sci. Technol.* **2003**, *37*, 877-891.

[93] Ziemann, P.; Atkinson, R. *Chem. Soc. Rev.* **2012**, *41*, 6582-6605.

[94] Peeters, J.; Nguyen, T. L.; Vereecken, L. *Phys. Chem. Chem. Phys.* **2009**, *11*, 5935-5939.

[95] Vereecken, L.; Peeters, J. *Phys. Chem. Chem. Phys.* **2010**, *12*, 12608-12620.

[96] Scheer, A. M.; Welz, O.; Zádor, J.; Osborn, D. L.; Taatjes, C. A. *Phys. Chem. Chem. Phys.* **2014**, *16*, 13027-13040.
[97] Lelieveld, J.; Butler, T. M.; Crowley, J. N.; Dillon, T. J.; Fischer, H.; Ganzeveld, L.; Harder, H.; Lawrence, M. G.; Martinez, M.; Taraborrelli, D.; Williams, J. *Nature*, **2008**, *452*, 737-740.
[98] Fuchs, H.; Hofzumahaus, A.; Rohrer, F.; Bohn, B.; Brauers, T.; Dorn, H-P.; Häseler, R.; Holland, F.; Kaminski, M.; Li, X.; Lu, K.; Nehr, S.; Tillmann, R.; Wegener, R.; Wahner, A. *Nature Geo.* **2013**, *6*, 1023-1026.
[99] Lockhart, J.; Blitz, M.; Heard, D.; Seakins, P.; Shannon, R. *J. Phys. Chem. A* **2013**, *117*, 11027-11037.
[100] Lockhart, J.; Blitz, M. A.; Heard, D. E.; Seakins, P. W.; Shannon R. J. *J. Phys. Chem. A* **2013**, *117*, 5407-5418.
[101] Peeters, J.; Müller, J. F. *Phys. Chem. Chem. Phys.* **2010**, *12*, 14227-14235.
[102] Yu, T.; Truhlar, D. G. *Chem. Sci.* **2011**, *2*, 2199-2213.
[103] Zheng, J.; Truhlar, D. G. *J. Chem. Theory and Comput*. **2013**, *9*, 1356-1367.